scientific reports

Check for updates

OPEN

Mineral states and sequestration processes involving soil biogenic components in various soils and desert sands of Inner Mongolia

Xuemei Yang[1,2], Xin Gao[2], Khan M. G. Mostofa[2]✉, Wang Zheng[2], Nicola Senesi[3], Giorgio S. Senesi[4], Davide Vione[5,6], Jie Yuan[7], Si-Liang Li[2], Longlong Li[2] & Cong-Qiang Liu[2]✉

Soil biogenic components are subject to continuous sequestration, and export from soils into the surrounding air and water environments. However, the processes involving the stability or lability of their mineral states remain still unclear. To assess these issues, we have measured various biogenic components in a number of agricultural, forest, grassland, and deep soils, as well as desert sands from Inner Mongolia, both in the solid state and liquid extracts. The contents of soil organic carbon (SOC) and soil total nitrogen (STN) were higher in soils than in sands, whilst those of soil total sulfur (STS) and inorganic carbon were higher in sands and deeper soils. The significant positive correlations found between STS and SOC, and STN, and their significant negative correlations with pH and δ^{13}C-SOC in all soils suggest a pH-dependent sequestration of C, N, and S. The decreased stability of organo-mineral complexes at acidic pH, resulting from the acidification of humic substance (HS) functionalities, leads to a higher availability of nutrients that facilitates the sequestration of soil organic matter (SOM). Conversely, an increase in pH enhances the stability of organo-mineral complexes by promoting negatively charged HS functionalities, which reduces the availability of nutrients and the sequestration of SOM. The δ^{13}C-SOC enrichment in desert sands (-17.63 to -7.10‰) and its depleted values in soils (-24.9 to -18.8‰) suggest the occurrence of C sequestration in desert, via uptake of enriched atmospheric CO_2 (-8.4‰). The fluorescence spectra of humic substance components and their molecular weights in sands were typically different from those of soils. The predominant relatively low molecular weight (MW) (< 15–25 kDa) of alkali-extracted (complexed state: CS) components and the relatively high MW (> 25 − 15 kDa) of water-extracted (labile state: LS) components of all soils suggest, respectively, their involvement in organo-mineral complexes and for export into the surrounding environment. The quantities of LS and CS soil components differ significantly on dependence of soil characteristics, implying their corresponding lability or stability in soils. These findings will provide useful input for the management of the corresponding soil/sand ecosystems.

Keywords Forest, agriculture, grassland and deep soils, Desert sands, Biogenic components (C, S, N and SiO_3^{2-}), Humic substances, Nutrients, High performance size exclusion chromatography

Abbreaviations

LS	Labile state, i.e. water extracted fractions (W_e)
CS	Complexed state, i.e. alkali extracted fractions (A_e)
DIC	Dissolved inorganic carbon
DIN	Dissolved inorganic nitrogen
DIP	Dissolved inorganic phosphorous

[1]Institute of Ecology, College of Urban and Environmental Sciences, Peking University, Beijing, China. [2]School of Earth System Science, Tianjin University, 92 Weijin Road, Tianjin 300072, China. [3]Dip.to di Scienze del Suolo, della Pianta e degli Alimenti, Università degli Studi di Bari "Aldo Moro", Via G. Amendola 165/A, 70126 Bari, Italy. [4]CNR - Istituto per la Scienza e Tecnologia dei Plasmi (ISTP), sede di Bari Via Amendola, 122/D, 70126 Bari, Italy. [5]Dipartimento di Chimica, Università degli Studi di Torino, Via P. Giuria 5, 10125 Torino, Italy. [6]Centro Interdipartimentale NatRisk, Via Leonardo da Vinci 44, 10095 Grugliasco, TO, Italy. [7]College of Resources and Environment, Xingtai University, Quanbei East Road 88, Qiaodong District, Xingtai City, Hebei Province, China. ✉email: mostofa@tju.edu.cn; liucongqiang@tju.eu.cn

DOC	Dissolved organic carbon
DOC_{LS}	LS DOC
DOC_{CS}	CS DOC
DOC_{LS+CS}	LS and CS DOC
DOM	Dissolved organic matter
DON	Dissolved organic nitrogen
DTN_{LS}	LS dissolved total nitrogen
DTN_{CS}	CS dissolved total nitrogen
F_{int}	Fluorescence intensity
FA	Fulvic acids
FA_{LS+CS}	LS and CS FA
HA	Humic acids
HA_{LS+CS}	LS and CS HA
HPSEC	High performance size exclusion chromatography
HS	Humic substances
HS_{LS+CS}	LS and CS HS
M_n	Number average molecular weight
M_w	Weight average molecular weight
MW	Molecular weight
PLS_{LS+CS}	LS and CS PLS
SOC	Soil/Sand organic carbon
STH	Soil/Sand total hydrogen
STN	Soil/Sand total nitrogen
STS	Soil/Sand total sulfur
$SO_4^{2-}{}_{LS+CS}$	LS and CS SO_4^{2-}

Soil organic matter (SOM), and especially its humic substance (HS) fractions, play multiple fundamental functions in soils and sands, which include: formation of organo-mineral complexes[1,2]; soil structure, cation exchange capacity and buffer/water-holding capacity[3,4]; oxygenic/anoxygenic photosynthesis[5,6] via uptake or sequestration of carbon[7,8], nitrogen[9,10], and sulfur[11–13]; microbial mineralization of HS or SOM[2,14] with emission of CO_2[15,16], N_2, or N_2O[17,18], and COS and H_2S[19], as well as export of water-soluble components (e.g. DOM, DIC, nutrients and various elements) via rainwater discharge and/or groundwater infiltration[20–23]. These biogeochemical processes constantly fuel the microbial food chains in downstream river-lake-marine environments[24]. Continuous export and/or emissions of various components from soils into the surrounding environments are counterbalanced by their sequestration in soils/sands, particularly in the case of C, N, and S. These sequestration processes in soils and desert sands remain unclear.

The mineralization of organic components in soil and sand primarily occurs at the mineral-microbes/organic interfaces[2,25] via microbial heterotrophic respiration[14]. In this framework, labile state (LS) components, or lability, refer to the fresh, soluble organic molecules derived from decaying plant materials, as well as readily available byproducts produced from various soil minerals under specific environmental conditions[26–28]. These components are not bound in organo-mineral complexes and are thus susceptible to export into the surface water and groundwater of the surrounding environment. However, some key degraded byproducts can form organo-mineral complexes that remain in the complexed state (CS), or stability, in soil and sand[28–31]. However, the generation of LS and CS forms of soil or sand components under environmental conditions and their correlations among themselves, and with other components, remain unclear. Furthermore, HS fractions, i.e., humic acids (HA), fulvic acids (FA), and protein-like substances (PLS) primarily contribute to these processes by either exporting or stabilizing components as organo-minerals[22,27,28,32]. However, it is still unclear which molecular weight (MW) fractions of HA, FA, and PLS are involved in either the lability and export into surface water and groundwater, or in their stability.

Based on the above considerations, we isolated a water extractable fraction (W_e, containing the LS fraction) and an alkali extractable fraction (A_e, CS fraction) from soils with different land uses (forest, agriculture, grassland) and at different depths (superficial and deep layers), and from desert sands. The key objectives of this study were to: *(i)* assess the occurrence of SOC and its stable isotopes (δ^{13}C-SOC), and their relation with soil and sand total sulfur (STS), soil/sand inorganic carbon (SIC), and soil and sand total nitrogen (STN), in order to infer their roles in the sequestration of C, S, or N, and mineral neformation; (*ii*) measure the occurrence of both LS and CS components, including dissolved organic carbon (DOC), HS fractions, dissolved inorganic carbon (DIC), SO_4^{2-}, dissolved N-nutrients, dissolved organic nitrogen (DON), PO_4^{3-}, dissolved organic phosphorus (DOP) and dissolved SiO_3^{2-}, to assess their simultaneous role in lability and export, or stability in organo-mineral complexes; (*iii*) investigate the lability and export, or stability role of HS fractions by high performance size-exclusion chromatography (HPSEC), and *(iv)* comprehensively assess the key factors that affect the LS and CS fractions in soils and sands.

Results

Biogeochemical occurrence, mineral states and sequestration of soil/sand components

Organic and inorganic C plus δ^{13}C-SOC

The SOC content featured a large variation (from 0.21 to 16.7 g/kg) among soil types, with the highest average value in agricultural soils (12.8 ± 3.0 g/kg). It was, respectively, 7.5%, 137%, 1836%, and 3278% higher than that in forest, grassland, deep soils, and desert sands (Table 1, S1). The SOC contribution to STC showed a similar order: agricultural soils (70.0 ± 15.3%) > forest soils (64.0 ± 21.1%) > grassland soils (27.7 ± 9.3%) > desert sands

Soil type	pH	EC	Water content	STC	SOC	SIC	STS	STN	C/*N*	SOC/S	δ^{13}C-SOC	$\delta^{15}N$	Soil texture[a]		
		µS cm^{-1}	(%)	g kg^{-1}	g kg^{-1}	g kg^{-1}	g kg^{-1}	g kg^{-1}			‰	‰	%	%	%
Forest ($n=4$)	8.17 ± 0.29	68.2 ± 28.1	2.16 ± 1.35	18.9 ± 2.1	11.9 ± 3.5	7.0 ± 4.3	0.204 ± 0.007	1.51 ± 0.59	17.3 ± 10.0	155 ± 42	−23.8 ± 0.9	6.21 ± 0.86	51.67 ± 33.96	44.71 ± 30.66	3.6 ± 3.3
Agriculture ($n=4$)	8.28 ± 0.14	250 ± 327	2.62 ± 1.24	18.5 ± 2.5	12.8 ± 3.0	5.6 ± 2.9	0.221 ± 0.012	1.34 ± 0.26	16.6 ± 4.0	155 ± 34	−23.5 ± 1.4	5.00 ± 1.69	66.81 ± 30.4	31.69 ± 29.03	1.48 ± 1.38
Grassland ($n=4$)	8.79 ± 0.30	62.1 ± 12.5	1.32 ± 1.13	19.1 ± 15.5	5.4 ± 4.2	13.7 ± 11.5	0.192 ± 0.017	0.77 ± 0.70	33.3 ± 10.0	72 ± 52	−20.1 ± 0.9	4.29 ± 0.19	84.47 ± 1.14	15.01 ± 0.98	0.53 ± 0.16
Desert ($n=5$)	8.60 ± 0.08	30.8 ± 9.1	0.22 ± 0.16	2.7 ± 1.2	0.38 ± 0.19	2.3 ± 1.0	0.177 ± 0.006	0.10 ± 0.02	35.8 ± 23.6	5.6 ± 2.6	−11.4 ± 5.1	nd	99.32 ± 1.41	0.654 ± 1.384	0.10 ($n=1$)
Deep ($n=3$)	8.36 ± 0.22	65.2 ± 17.2	1.70 ± 0.96	14.2 ± 8.2	0.66 ± 0.40	13.6 ± 8.1	0.198 ± 0.006	0.79 ± 0.30	20.8 ± 7.0	9.0 ± 5.6	−23.7 ± 1.0	3.50 ± 1.02	75.4 ± 5.9	23.49 ± 5.56	1.14 ± 0.34
Mean	8.47	98.64	1.50	14.1	7.2	6.88	0.20	0.88	22.6	79.2	-19.2	5.25	76.97	21.70	1.33
Range	7.90–9.21	23.8–740	0.10–4.4	1.6–41.0	0.21–16.7	1.4–30.4	0.18–0.24	0.07–1.74	9.6–65.5	3.0-200	-24.9 to -7.1	3.15–7.13	18.52–99.99	0-74.67	0.0-6.77

Table 1. Average chemical and physical properties of the forest, agricultural, grassland and deep soils, and desert sands examined.

(14.3 ± 3.0%) > deep soils (5.1 ± 3.8%). These findings suggest that agricultural and forest soils acted as primary storage/sequestration sites of SOC originating from plant materials, whereas the lowest content of SOC in deep soils would be due to its degradation.

Differently, SIC showed the highest average content in grassland soils (13.7 ± 11.5 g/kg), which was very similar to that in deep soils (only ~ 1.2% higher), and approximately 94.0%, 141%, and 487% higher than, respectively, forest soils, agricultural soils, and desert sands. The SIC contribution to STC followed a similar order, on average: deep soils (95.0 ± 3.8%) > desert sands (85.7 ± 3.0%) > grassland soils (72.3 ± 9.3%) > forest soils (36.0 ± 21.1%) > agricultural soils (30.2 ± 15.3%).

The δ^{13}C-SOC varied from − 24.85‰ to -7.10‰, with very similar and low average values detected in forest, agricultural, and deep soils (respectively, -23.77 ± 0.88‰, -23.53 ± 1.41‰, and − 23.66 ± 1.04‰). Slightly higher values were found in grassland soils (-20.05 ± 0.9‰) and, especially, in desert sands (-11.37 ± 5.05‰). Similar δ^{13}C-SOC values have been reported in top and deep forest and agricultural soils[33–35].

The average contents of DOC_{LS} and DOC_{CS} in agricultural soils (173 ± 64 and 571 ± 161 mg/kg, respectively) were higher than in forest soils (by 12.0% and 10.3%, respectively), grassland soils (by 19.0% and 166%, respectively), deep soils (by 108% and 78.0%, respectively), and desert sands (by 1215% and 580%, respectively; Fig. 1; Table 2). Noteworthy, grassland soils showed a relatively low content of DOC_{CS} in comparison with agricultural and forest soils (respectively, 166% and 141% lower). Conversely, grassland soils featured a relatively high content of DOC_{LS}, exceeding agricultural and forest soils by 19.0% and 6.0%, respectively, which was likely due to the presence of grassland vegetation. Grasslands might thus be minor contributors to organo-mineral stability. In particular, the average DOC_{LS} and DOC_{CS} contributions to SOC followed the order: deep soils (respectively, 15.0 ± 8.5% and 56.4 ± 25.6%) > desert sands (respectively, 3.3 ± 0.92% and 17.8 ± 12.6%) > grassland soils (respectively, 3.3 ± 2.1% and 4.7 ± 1.4%) > forest soils (respectively, 1.3 ± 0.67% and 5.3 ± 4.8%,) > agricultural soils (respectively, 1.4 ± 0.7% and 4.6 ± 1.6%). Various land uses thus show a diversity in soil DOM lability that, in turn, indicates different organo-mineral stability in the corresponding soil types. In particular, deep soils typically showed the highest levels of lability and organo-mineral stability, presumably due to intense SOC mineralization upon long-term burial. Differently, forest soils > agricultural ≈ grassland (in the order) exhibited a relatively higher CS organo-mineral stability, possibly due to HS or DOM primarily derived either from plant litters or from photosynthetic SOC in forest soil compared to those of agriculture or grassland[29,31,36].

DIC_{LS} and DIC_{CS} (Fig. 1; Table 2) showed the highest average contents in agricultural soils (111 and 910 mg/kg), which were higher compared to forest soils (by, respectively, 11.0% and 42.0%) > grassland soils (by, respectively, 27.2% and 36.3%,) > desert sands (by, respectively, 38.0% and 56.0%). In particular, deep soils showed the highest DIC_{LS} content among all soils (30.0% higher than agricultural soils), but their DIC_{CS} content was 36.0% lower than for agricultural soils (Fig. 1).

Furthermore, forest soils ≈ grasslands ≈ deeper soils > desert sands (in the order) exhibited relatively similar levels of DIC_{CS}-induced mineral neoformation. In particular, the DOC_{LS} and DOC_{CS} values in desert sands (lower by, respectively, 1216% and 580% compared to agricultural soils) and the DIC_{LS} and DIC_{CS} content (respectively, 38% and 56% lower than in agricultural soils) would primarily arise from atmospheric CO_2 uptake by sand photosynthetic microorganisms[8,37,38]. These processes would subsequently lead to the generation of HS/DOM[8,37,38] and their simultaneous mineralization via photoinduced production of reactive oxygen species[39]. It would follow production of DIC_{LS} and DIC_{CS}, lability of LS forms, and sequestration in CS forms via neoformation of carbonate minerals as discussed before. The highly enriched δ^{13}C-SOC (-11.37 ± 5.05‰) would further support the uptake of atmospheric CO_2 by photosynthetic microorganisms in desert sands.

Fluorescence features of HS components

Up to three HS_{LS} and HS_{CS} components (HA_{LS} and HA_{CS}, FA_{LS} and FA_{CS}, as well as PLS_{LS} and PLS_{CS}), together with their degradative fluorescent components as byproducts or residues were identified by the EEM-PARAFAC in HS from all soils, which are similar to earlier studies[22,28,40]. Both HS_{LS} and HS_{CS} isolated from forest soils featured three components with only the long-wavelength peaks (T and M) of PLS_{LS} being degraded, whereas all the other components (HA_{LS} and HA_{CS}, FA_{LS} and FA_{CS}, as well as PLS_{CS}) were non-degraded or unaffected by environmental conditions (Fig. 2; Table S2), as shown in an earlier study[28]. Noteworthily, the higher fluorescence intensity (F_{int}) of peak M compared to peaks C and T in both LS- and CS-forms of FA from forest soils, along with the fact that F_{int} of LS showed the highest contribution among all soils (Fig. 3).

Agricultural soils exhibited two HS_{LS} components, i.e., degraded HA_{LS} with two peaks and degraded PLS_{LS} with two short-wavelength peaks (T_{UV} and A), as well as three HS_{CS} components that were mostly unaffected by environmental factors (Fig. 2; Table S2). This issue suggests that human activities influenced HS_{LS} components, but HS_{CS} remained unaffected. A similar highly degradative nature of HS_{LS} components in agricultural soils was reported elsewhere[28,41]. Furthermore, the HA peak C in the LS- and CS-forms of agricultural soils showed, on average, the highest (LS) and the lowest (CS) F_{int} values among all soil types (Fig. 3). This might happen because human and environmental factors (e.g., ploughing, sunlight) would increase the HA_{LS} content with a corresponding decrease of CS forms from which LS might derive, and also increase the FA_{CS} contribution to organo-minerals (Fig. 3). The extended mineralization of HS_{LS} and HA_{CS} components might be responsible for the high generation of DIC_{LS} and DIC_{CS} in agricultural soils (Fig. 1). Furthermore, PLS_{LS} from agricultural soils exhibited the second highest F_{int} among all soil types, which might also be ascribed to human activities[42]. These processes would finally lead to leaching or export of HA_{LS} and PLS_{LS} from agricultural soils into the surrounding ecosystems, e.g., surface water and groundwater.

Grassland soils showed three HS components in LS- and CS-forms, which is identical to forest soils (Fig. 2). These results would suggest the occurrence of very similar processes in both soil types. In particular, HS components might be freshly originated from grassland vegetation and anoxygenic photosynthetically-derived SOC under wet conditions, and might remain mostly in a non-degraded state under low temperatures and

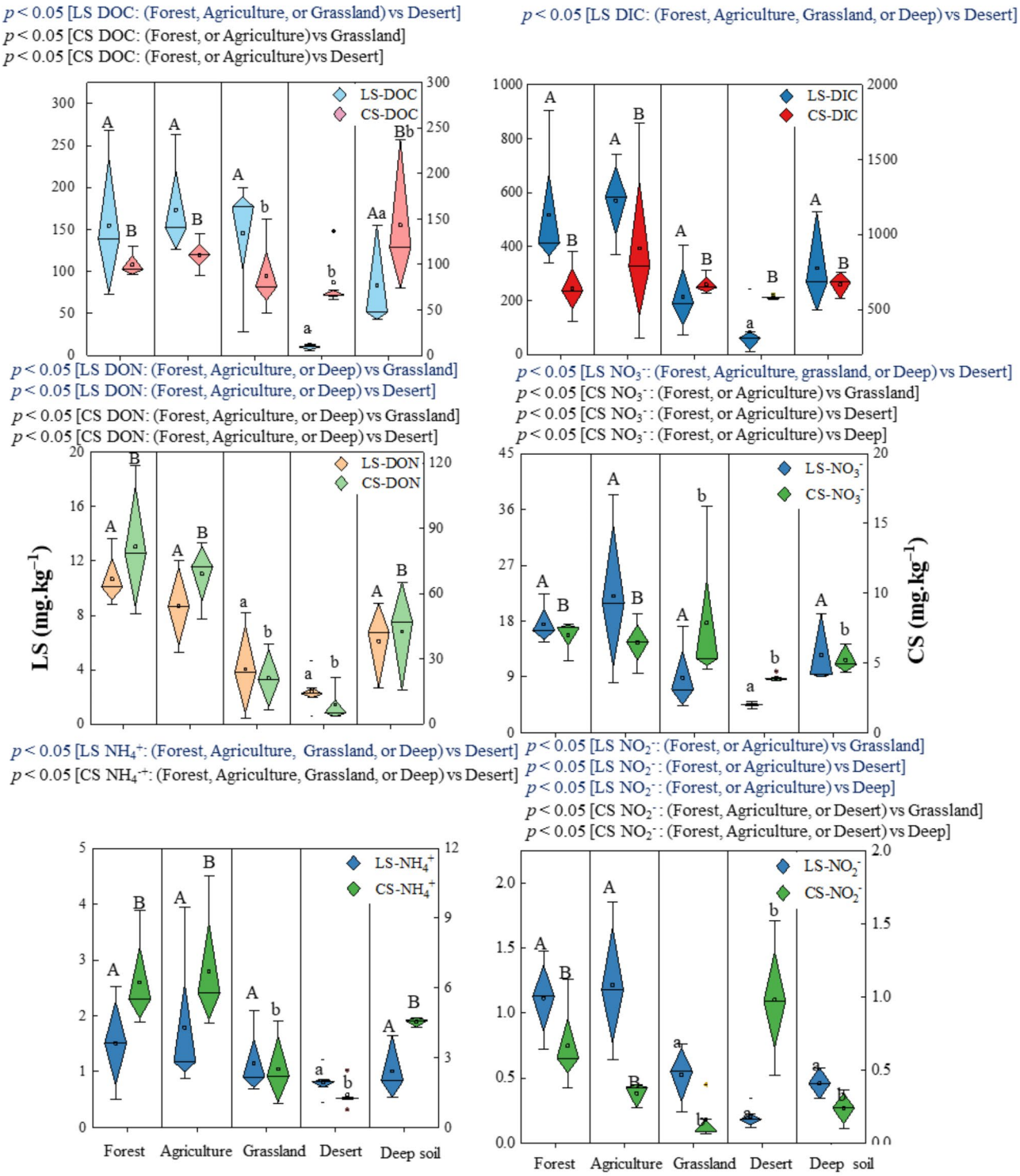

Fig. 1. Concentrations of labile state (LS) and complexed state (CS) dissolved organic carbon (DOC_{LS} and DOC_{CS}), dissolved inorganic carbon (DIC_{LS} and DIC_{CS}), dissolved organic nitrogen (DON_{LS} and DON_{CS}), nitrate ($NO_3^-{}_{LS}$ and $NO_3^-{}_{CS}$), ammonium ($NH_4^+{}_{LS}$ and $NH_4^+{}_{CS}$), and nitrite ($NO_2^-{}_{LS}$ and $NO_2^-{}_{CS}$) in forest, agricultural, grassland and deep soils and desert sands. Different lower case and capital letters (**A**, **B** or **a**, **b**) indicate significant differences at $p < 0.05$ level.

Sample type	DOC	DIC	SO_4^{2-}	TN	DIP	NO_2^{-}-*N*	NH_4^{+}-*N*	NO_3^{-}-*N*	DON	TP	DOP	SiO_3^{2-}-Si
	mg.kg	mg.kg	mg.kg	mg.kg	mg.kg	mg.kg	mg.kg	mg.kg	mg.kg	mg.kg	mg.kg	mg.kg
Labile state (LS: water extracts), or lability of soil components												
Forest soil	154.6 ± 96.6	99.6 ± 14.5	27 ± 29.7	30.8 ± 6.5	3.6 ± 3.9	1.1 ± 0.3	1.5 ± 0.9	17.5 ± 3.5	10.7 ± 2.2	5.9 ± 4.4	2.3 ± 0.6	44.3 ± 3.9
Agricultural soil	173.2 ± 64.3	110.6 ± 18.8	248.1 ± 445.5	33.7 ± 10.1	9.5 ± 9	1.2 ± 0.5	1.8 ± 1.4	22 ± 14	8.7 ± 3.4	11.8 ± 9.7	2.3 ± 0.7	33.4 ± 19.9
Grassland soil	145.7 ± 79.1	87 ± 44.2	11.6 ± 13.2	14.6 ± 9.7	1.7 ± 0.9	0.5 ± 0.2	1.2 ± 0.7	8.9 ± 6	4 ± 3.8	3.4 ± 1.6	1.6 ± 0.6	31.1 ± 5.8
Desert sand	13.2 ± 9.6	80.2 ± 31.8	6.6 ± 4.3	7.9 ± 2	1.2 ± 0.6	0.2 ± 0.1	0.8 ± 0.3	4.5 ± 0.4	2.4 ± 1.5	1.7 ± 1	0.5 ± 0.5	17.7 ± 2.1
Deep soil	83.2 ± 62.3	143.3 ± 84.1	29.6 ± 5.6	20.1 ± 6.6	0.9 ± 0	0.5 ± 0.1	1 ± 0.6	12.5 ± 5.7	6.1 ± 3.1	2.2 ± 0.4	1.3 ± 0.4	29.4 ± 5.6
*Complexed state (CS: alkali extracts), or stability of soil components***												
Forest soil	517.4 ± 260.5	640.8 ± 191.8	18.5 ± 7.6	95.9 ± 36.1	2.6 ± 1.2	1 ± 0.4	6.2 ± 2.2	7 ± 1.2	81.7 ± 32.9	11.7 ± 4.4	9.1 ± 4.6	352.3 ± 58.5
Agricultural soil	570.8 ± 161.5	909.5 ± 620.1	10.1 ± 2.3	83 ± 16.9	5.1 ± 3.3	0.7 ± 0.3	6.7 ± 2.9	6.5 ± 1.8	69.1 ± 15.9	13.9 ± 5.4	8.7 ± 2.3	278.6 ± 134.3
Grassland soil	214.4 ± 143.3	667.5 ± 69	24.5 ± 12.7	31.7 ± 21.7	1.6 ± 0.7	0.2 ± 0.1	2.5 ± 1.7	7.9 ± 5.6	21.1 ± 15.4	5.9 ± 3.1	4.3 ± 3.5	232.8 ± 61.8
Desert sand	84 ± 94.4	582.1 ± 13.6	20.7 ± 6.1	14.5 ± 8.6	3.2 ± 2.1	0.2 ± 0.1	1.4 ± 0.6	3.9 ± 0.3	9 ± 7.7	4.1 ± 2.5	0.9 ± 0.8	195.5 ± 8.3
Deep soil	320.4 ± 187.3	668.5 ± 89.4	12.6 ± 6.5	52.7 ± 26.1	2 ± 1	0.3 ± 0.1	4.5 ± 0.2	5.2 ± 1.0	42.6 ± 25.2	7.3 ± 4.1	5.3 ± 3.9	263.1 ± 100.4

Table 2. Average contents of labile state (LS: water extracts, or lability)*, and complexed state (CS: alkali extracts, or stability)** DOC, DIC, SO_4^{2-}, and various nutrients in the forest, agricultural, grassland, and deep soils, and desert sands examined. ***Definition**: Labile state (LS), or lability, is operationally defined as the net amount of water-soluble soil components extracted by water from the soil. Lability, or LS, typically refers to the fresh, soluble organic molecules derived from decaying plant materials, as well as readily available byproducts produced from various soil minerals under specific environmental conditions at the mineral-microbes interfaces. These components are not bound in organo-mineral complexes and are therefore susceptible to export into the surrounding environment through water and rainwater discharges. A low amount of LS soil components indicates low lability, while a high amount indicates high lability. For instance, lability, or LS of DOC (DOC_{LS}) varies from 0.31 to 13.4 mg/L for all soils and sands. ****Definition**: Complexed state (CS), or stability, is operationally defined as the net amount of water-insoluble and alkali-soluble soil components extracted by alkali (0.1 N NaOH solution) from the soil. This typically refers to the water-insoluble complexed-state fractions of soil organo-mineral complexes that are not water-soluble and, therefore, are not susceptible to export into the surrounding environment through water and rainwater discharges. A low amount of CS soil components indicates a low stability (e.g. organo-, carbonate, silicate or secondary minerals), while a high amount indicates high stability. For instance, the stability, or CS of DOC (DOC_{CS}) varies from 0.53 to 45.2 mg/L for all soils and sands. Specifically, DOC_{CS} values are typically significantly higher, ranging from approximately 1.26 to 14.0 times (with an average of 4.42 ± 3.82 times) than DOC_{LS} values across all soil types, except for one grassland sample (site IM-12), where DOC_{CS} is lower (18.8%) than DOC_{LS}. This discrepancy is attributed to substantially higher DIC_{CS} values, which are 13.4 times lower than DIC_{LS}.

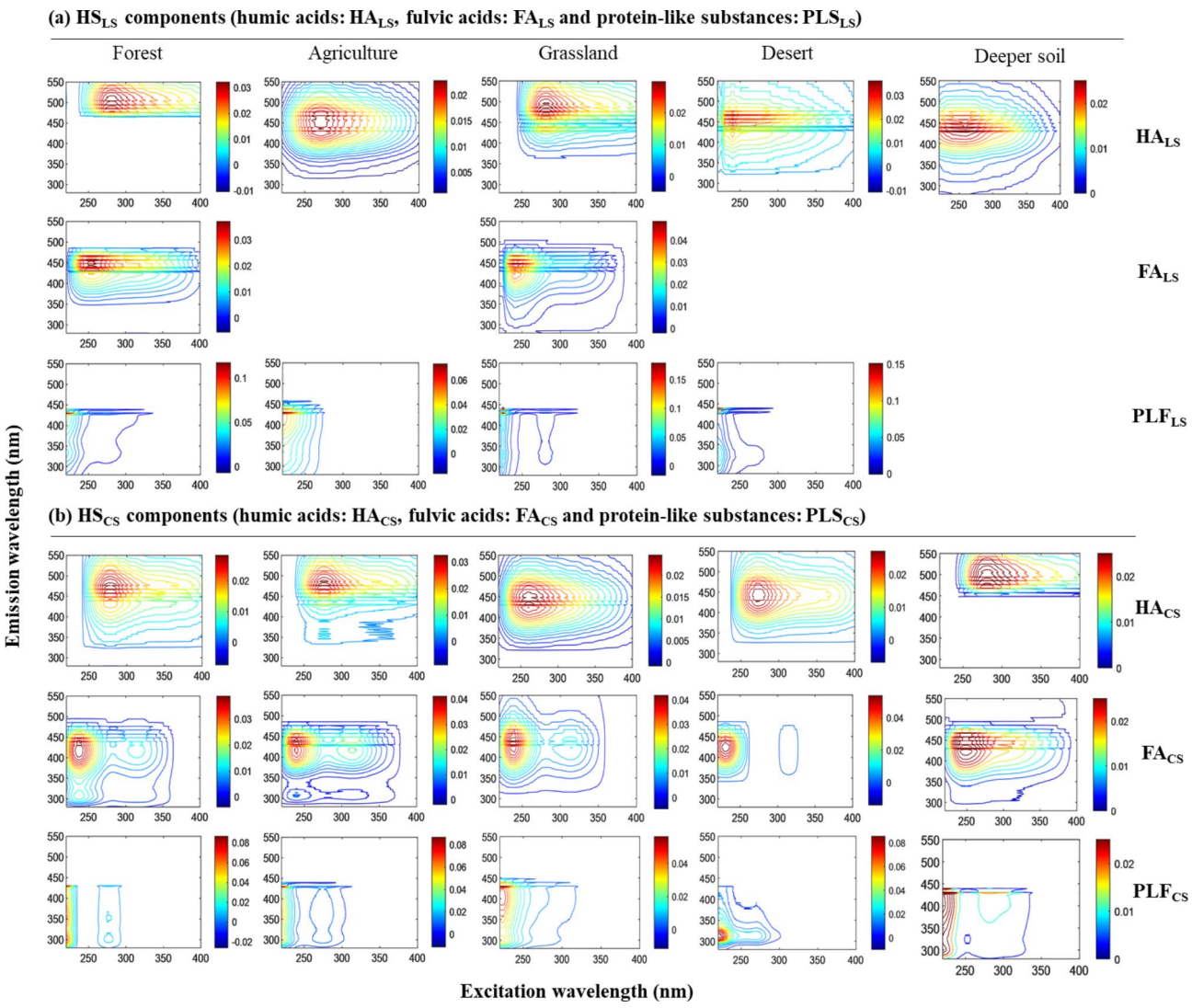

Fig. 2. Fluorescence (excitation-emission matrix, EEM) spectra of water-extracted/labile state (LS) humic substances (HS_{LS}) (**a**), and alkali-extracted/complexed state (CS) HS (HS_{CS}) (**b**) from forest, agricultural, grassland, and deep soils and desert sands. The HS components include humic acid-like (HA-like), fulvic acid-like (FA-like) and protein-like substances-like (PLS-like) identified using EEM-PARAFAC modeling of detected fluorescence peaks.

intense precipitations or wet conditions. In grassland soils the F_{int} of HA peak C, FA peak M, and PLS peak T of the CS-form were, on average, higher than for the corresponding LS-forms. Furthermore, HA_{CS} exhibited the most intense peak C among all soil types. These results would suggest a high contribution of all three HS components to organo-mineral complexes (Fig. 3). Simultaneously the three HS_{LS} components, freshly derived from grassland vegetation under environmental conditions (Fig. 2), would contribute to a high level of DOC_{LS} that might subsequently be exported to the surrounding environments via rainwater discharge from the grassland ecosystem.

Desert sands featured two HS_{LS} components that could be attributed to degraded HA_{LS} and degraded PLS_{LS} (Fig. 2; Table S2), as well as three HS_{CS} components, i.e., HA_{CS}, FA_{CS}, and PLS_{CS}, which could be assigned to relatively degraded states. In fact, the peaks of HA_{CS} and FA_{CS} were at shorter wavelengths than those of forest soils (Table S2), as also observed in a previous study[28]. The two peaks (270/312 nm and 220/312 nm) of PLS_{CS} might be mainly attributed to tyrosine-like substances (TYLS) (Fig. 2; Table S2)[18]. The highly degradative nature of HS_{LS} and partly of HS_{CS} components in desert sands might be due to the action of photochemically produced ROS[39]. In particular, the HS components in desert sands would primarily originate from photo-microbial respiration of photosynthetically-derived sand microorganisms, due to the absence of plant materials[8,37,38], in a condition similar to that occurring for aquatic planktonic microorganisms[18,43,44]. The detection of TYLS in desert sands[18] is different from the soils examined in this and earlier studies[22,28]. Moreover, the photochemical degradation of HS_{LS} and HS_{CS} components in desert sands was further supported by the relatively low F_{int} of HA_{LS} peak C and PLS_{LS} peak T, and would be caused by constant sunlight exposure in the absence of plants

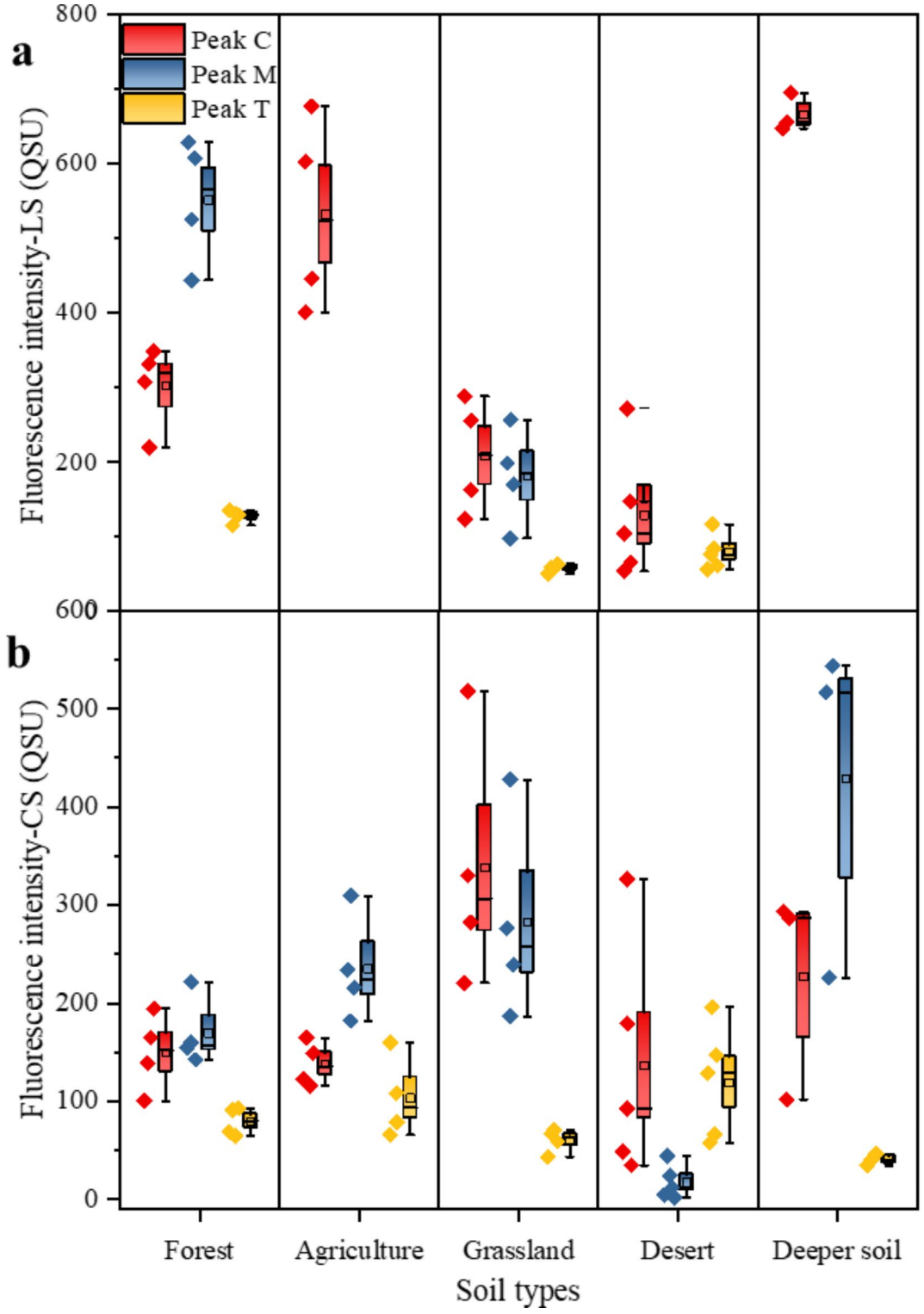

Fig. 3. Fluorescence intensities of humic acid (HA)-like peak C, fulvic acid (FA)-like peak M and protein-like substances-like peak T of water-extracts (labile state, LS) (**a**), and alkali-extracts (complexed state, CS) (**b**) from forest, agricultural, grassland, and deep soils and desert sands. The corresponding peaks (C, M and T) are shown in Fig. 2.

together with the lack of leaching or export via rainwater discharge/runoff from desert sands to the surrounding environments.

Finally, deep soils exhibited only one degraded HA_{LS} component with two peaks (C and A), occurring at relatively shorter wavelengths than the corresponding peaks of forest and agricultural soils[28], but showing

the highest F_{int} among all soil types (Fig. 3). Furthermore, deep soils featured three HS_{CS} components at very similar wavelengths as those of forest and agricultural soils, which would suggest that HS_{CS} in organo-minerals remained in a non-degraded state via organic carbon stabilization, together with the complete mineralization of FA_{LS} and PLS_{LS} components. Noteworthily, the highest F_{int} of FA_{CS} peak M and the lowest F_{int} of PLS_{CS}, which exhibited a highly microbially degradative nature in deep soils, along with the relatively high F_{int} of HA_{CS} peak C, would suggest a high contribution of organo-mineral complexes to organic C stabilization[1,2,45].

Overall, the wavelengths of peak A of HA_{LS} and HA_{CS} varied widely among the soil types studied, e.g. 280/505,495 and 280/477,486,460 nm for forest soils, as well as 260/430,439,448 and 280/495,505,477 nm for deep soils (Fig. 2; Table S2), which suggests the involvement of different functional groups[36,46,47]. Similarly, the wavelength of peak C of HA_{LS} and HA_{CS} also varied between forest soils (e.g. 355,380/505,495 and 350,375/477 nm) and grassland soils (e.g. 340,355,385/486 and 310,350/442 nm), which implies the occurrence of diverse functional groups. In particular, these groups would be primarily responsible for complexation with diverse metals[47,48], mostly via π–d electron bonding systems[40], with formation of organo-mineral complexes that result in the sequestration/stabilization of organic carbon in the soil matrix[40].

Characteristics of molecular weights of soil DOM components

The M_n and M_w values of HS components were determined by HPSEC and are listed in Table 3, S4. The DOM elution curves showed similar trends for all soils, exhibiting a total of 2 to 5 peaks, and the M_W distribution of their components ranged from 1 kDa to 35 kDa. In particular, three M_W fractions, i.e., large (M_W > 25 kDa), medium (M_W 25 kDa–15 kDa), and small (M_W < 15 kDa) are distinguished. The fraction with M_w > 25 kDa was particularly rich in LS-forms (1.9–66.0%) compared to CS-forms (1.3–3.9%), in which case the large M_w fraction was only detected in seven samples (Table 3, S4). On average, the percentage of DOM components with M_w > 25 kDa in LS-forms followed the order: desert sands (40 ± 25%) > grassland soils (5.0 ± 2.2%) > deep soils (3.0 ± 0.9%) > forest soils (3.0 ± 0.7%) > agricultural soils (3.0 ± 0.3), whereas the order in CS-forms was: deep soils (3.0 ± 1.3%) > grassland soils (2.0 ± 0.9%) > forest soils (2.2%) > desert sands (2.0%). In particular, the high M_w of LS-forms from desert sands might be ascribed to degraded HA_{LS}, which is also shown by EEM-PARAFAC analysis. Differently, the high M_w of CS-forms mostly exhibited by deep and grassland soils might be ascribed to the relatively higher contents of HA_{CS} and FA_{CS} in non-degraded state (Figs. 2 and 3).

The fraction exhibiting M_w between 15 and 25 kDa showed, on average, slight differences among the soils under study, except for desert sands, and followed the order: deep soils (96.4 ± 0.9%) > forest soils (96.1 ± 0.7%) > agricultural soils (95.4 ± 0.4%) > grassland soils (94.0 ± 1.6%) > desert sands (76.0 ± 28.0%) for DOM_{LS}, whereas for DOM_{CS} the order was: deep soils (94.2 ± 0.9%) > agricultural soils (92.4 ± 1.4%) > grassland soils (92.4 ± 0.6%) ≈ forest soils (92.3 ± 0.7%) > desert sands (90.4 ± 10.3%). Furthermore, DOM_{LS} components exhibited, on average, higher M_n and M_w (25211 ± 2826 and 25490 ± 2509 Da, respectively) compared to DOM_{CS} components (21051 ± 1551 and 22229 ± 1330 Da, respectively). The higher occurrence of DOM_{LS} components exhibiting M_w and M_n between 15 and 25 kDa, compared to DOM_{CS}, might be due to their high lability and/or hydrophilicity and to their possibly aliphatic nature[8,37,38]. In particular, the highest values for HS_{LS} were shown by desert sands (29085 ± 2189 and 29322 ± 2038 Da, respectively) and the lowest ones (23098 ± 292 and 24134 Da, respectively) by agricultural soils (Table 3, S4). This phenomenon would be due to the difference in DOM_{LS} sources, i.e., photosynthetically-derived SOC in desert sands[8,37,38] and plant -derived material in agricultural soils[29–31]. In the case of DOM_{CS}, the M_n and M_w values in deep soils (22437 ± 959 and 23563 ± 921 Da, respectively) were higher than those in desert sands (20447 ± 2758 and 21460 ± 2097 Da, respectively; Table 3, S4), probably because the three DOM_{CS} components remained in a non-degraded state due to their stabilization in organo-mineral complexes in deep soils (Fig. 2)[5,6,49,50]. In particular, the relatively low abundances of DOM_{CS} components in desert sands might be due to intense sunlight-induced photochemical degradation by ROS[39], which make reduce the stability of organo-mineral complexes and was further supported by the degraded states of the three DOM_{CS}, which exhibited peaks at EEM wavelengths that were shorter than in the other soil types (Fig. 2; Table S2).

Higher amounts of components with M_w < 15 kDa was measured in DOM_{CS} (3.1–23.7%, average: 7.3 ± 5.0%) compared to DOM_{LS} (0.6-2.0%, average: 1.4 ± 0.5%). These results are presumably due to the strong complexation properties of relatively low M_w components with various metals in soils, in comparison with high M_w components[39]. The content of the fraction with M_w < 15 kDa in DOM_{LS} followed, on average, the order: agricultural soils > grassland soils > forest soils > deep soils, and was completely absent in desert sands. The corresponding order for DOM_{CS} was: desert sands > agricultural soils > grassland soils > forest soils > deep soils. Specifically, the complete absence of the fraction with M_w < 15 kDa in DOM_{LS} of desert sands and its highest amount in DOM_{CS} would suggest that intense photochemical degradation by ROS[39] would be responsible for the complete degradation of DOM_{LS}, whereas the organo-mineral complexes of the corresponding DOM_{CS} components would be relatively less labile[46,51]. Differently, the highest content of the small M_w fraction in DOM_{LS} from agricultural soils might be ascribed to the degradation of organo-mineral complexes by the impact of human activities (e.g. ploughing, sunlight) on the uppermost soil, as discussed before.

STS, $SO_4^{2-}{}_{LS+CS}$, and $SOS + S_n^{2-}$

The STS contents ranged from 0.168 to 0.236 $g.kg^{-1}$ and, on average, showed a slight variation among the studied soil types, i.e., the highest value was measured in agricultural soils (0.221 ± 0.013) which was higher (by 8.0%) than that in forest soils > deep soils (12.0%) > grassland soils (15.0%) > desert sands (24.0%). Similarly, $SO_4^{2-}{}_{LS}$ varied from 1.86 to 916 $mg.kg^{-1}$ and showed, on average, a large variation with the highest content in agricultural soils (248 ± 446 $mg.kg^{-1}$), which was higher (by 738%) than in deep soils > forest soils (819%) > grassland soils (2040%) > desert sands (3650%) (Fig. 4). The highest STS and $SO_4^{2-}{}_{LS}$ contents in agricultural soils might be primarily responsible for the relatively high DOC_{LS}, DOC_{CS}, and DIC_{LS+CS} production and export[15,16,34] from

Soil type	Lability or LS M_n (Da)	Lability or LS M_w (Da)	ρ-MQ	> 25 kDa (%)	15–25 kDa (%)	< 15 kDa (%)	Stability or CS M_n (Da)	Stability or CS M_w (Da)	ρ-NaOH	> 25 kDa (%)	15–25 kDa (%)	< 15 kDa (%)
Forest ($n=4$)	23,896 ± 113	24,715 ± 43	1.03 ± 0.003	0.03 ± 0.007	0.96 ± 0.007	0.012 ± 0.001	20,836 ± 140	22,017 ± 165	1.05 ± 0.003	0.02	0.92 ± 0.007	0.071 ± 0.006
Agriculture ($n=4$)	23,098 ± 292	24,134 ± 258	1.04 ± 0.002	0.03 ± 0.003	0.95 ± 0.004	0.018 ± 0.002	20,888 ± 626	22,186 ± 695	1.06 ± 0	-	0.92 ± 0.014	0.076 ± 0.014
Grassland ($n=4$)	24,250 ± 1032	24,995 ± 637	1.03 ± 0.01	0.05 ± 0.022	0.93 ± 0.01	0.014 ± 0.004	20,993 ± 432	22,253 ± 504	1.06 ± 0.004	0.02 ± 0.01	0.92 ± 0.006	0.062 ± 0.01
Desert ($n=5$)	29,085 ± 2189	29,322 ± 2038	1 ± 0	0.40 ± 0.25	0.76 ± 0.28	-	20,447 ± 2758	21,460 ± 2097	1.05 ± 0.04	0.02	0.90 ± 0.10	0.121 ± 0.10
Deep ($n=3$)	24,605 ± 766	24,995 ± 482	1.01 ± 0.012	0.03 ± 0.009	0.96 ± 0.009	0.008 ± 0.003	22,437 ± 959	23,563 ± 921	1.05 ± 0.01	0.03 ± 0.013	0.94 ± 0.009	0.039 ± 0.012

Table 3. Average values of weight average molecular weight (M_W), and number average molecular weight (M_n) of dissolved organic matter (DOM) in labile state (LS: water-extracted) and complexed state (CS: alkali-extracted) from the forest, agricultural, grassland and deep soils, and desert sands examined.

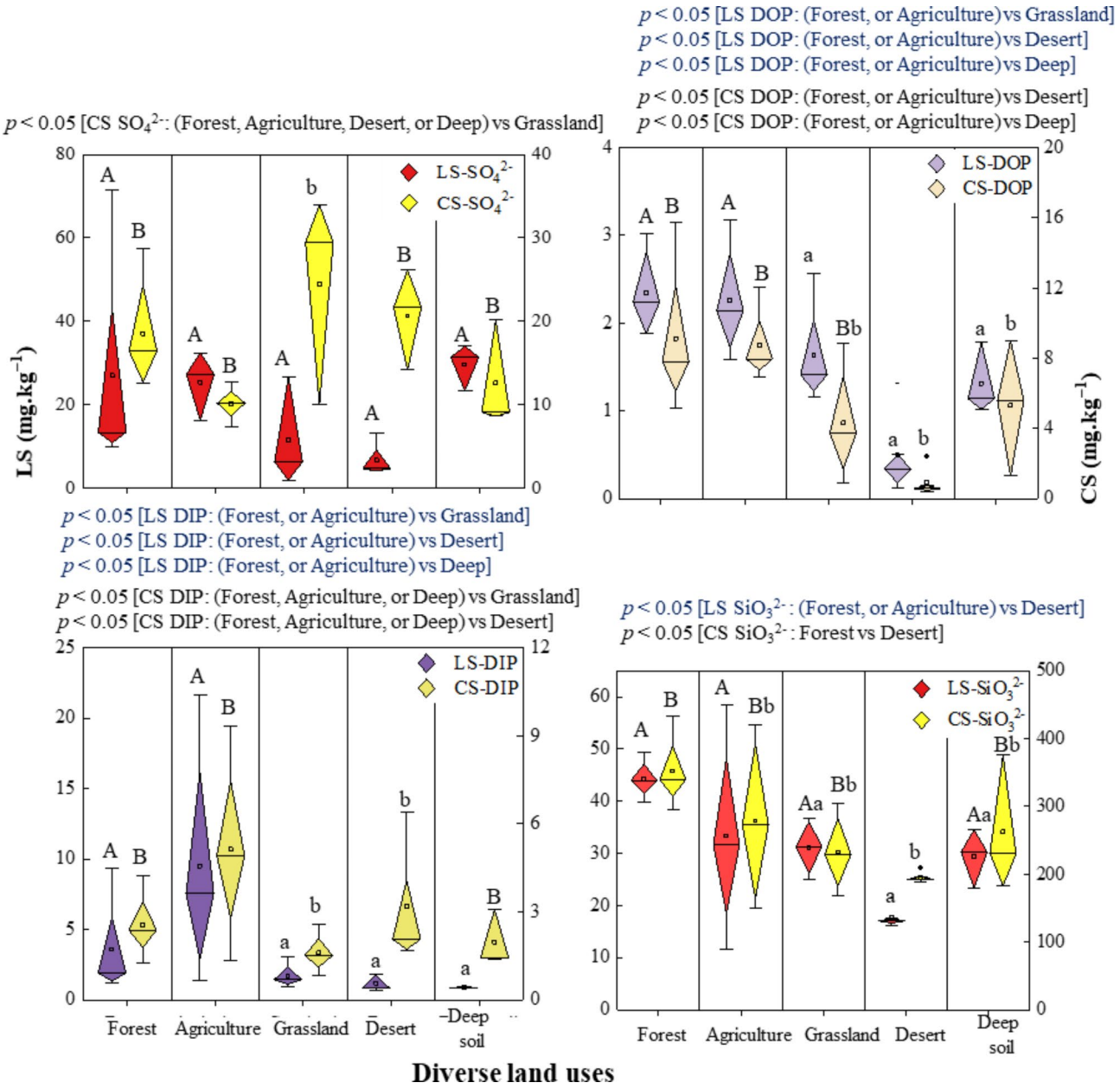

Fig. 4. Concentrations of labile state (LS) and complexed state (CS) sulfate ($SO_4^{2-}{}_{LS}$ and $SO_4^{2-}{}_{CS}$), dissolved organic phosphorus (DOP_{LS} and DOP_{CS}), dissolved inorganic phosphate (DIP or $PO_4^{3-}{}_{LS}$ and DIP or $PO_4^{3-}{}_{CS}$), and silicate ion ($SiO_3^{2-}{}_{LS}$ and $SiO_3^{2-}{}_{CS}$) in forest, agricultural, grassland and deep soils and desert sands. Different lower case and capital letters (A, B or a, b) indicate significant differences at $p < 0.05$ level.

the dissolution or mineralization of DOM-bound clay, carbonate and/or secondary minerals[2,52–54] via microbial sulfate reduction[55,56]. Differently, $SO_4^{2-}{}_{CS}$ ranged from 7.3 to 34.0 mg.kg^{-1} among all soils and showed the highest average content in grassland soils (24.0 mg.kg^{-1}), which was higher (by 19.0%) than desert sands > forest soils (32%) > deep soils (94%) > agricultural soils (142%) (Fig. 4). The highest occurrence of $SO_4^{2-}{}_{CS}$ in grassland soils might be primarily responsible for the high DOC_{CS} mineralization and subsequent production of relatively high DIC_{CS} (668 mg.kg^{-1}), which would end up in neoformation of carbonate minerals in soil[55,56].

Due to the small amounts of $SO_4^{2-}{}_{LS+CS}$, soil organic sulfur (SOS) plus sulfides (S_n^{2-}) contents were very similar to the STS content, showing the highest levels in agricultural soils (0.204 ± 0.012 g.kg^{-1}), which was slightly higher (by 7.8%) than that in forest soils > deep soils (11.0%) ≈ grassland soils (11.2%) > desert sands (18.4%). These results suggest that SOS + S_n^{2-} were the predominant forms of S in soils, and contributed approximately 93.0–96.0% to STS.

The significant positive correlations of STS with SOC, DOC_{LS}, or DOC_{CS} (Fig. 5; Table S3) suggest that the major STS fractions were partly derived from DOM and SOC-bound microorganisms. This result was further supported by the positive correlations of STS with STN and STH, which are primarily related to SOC

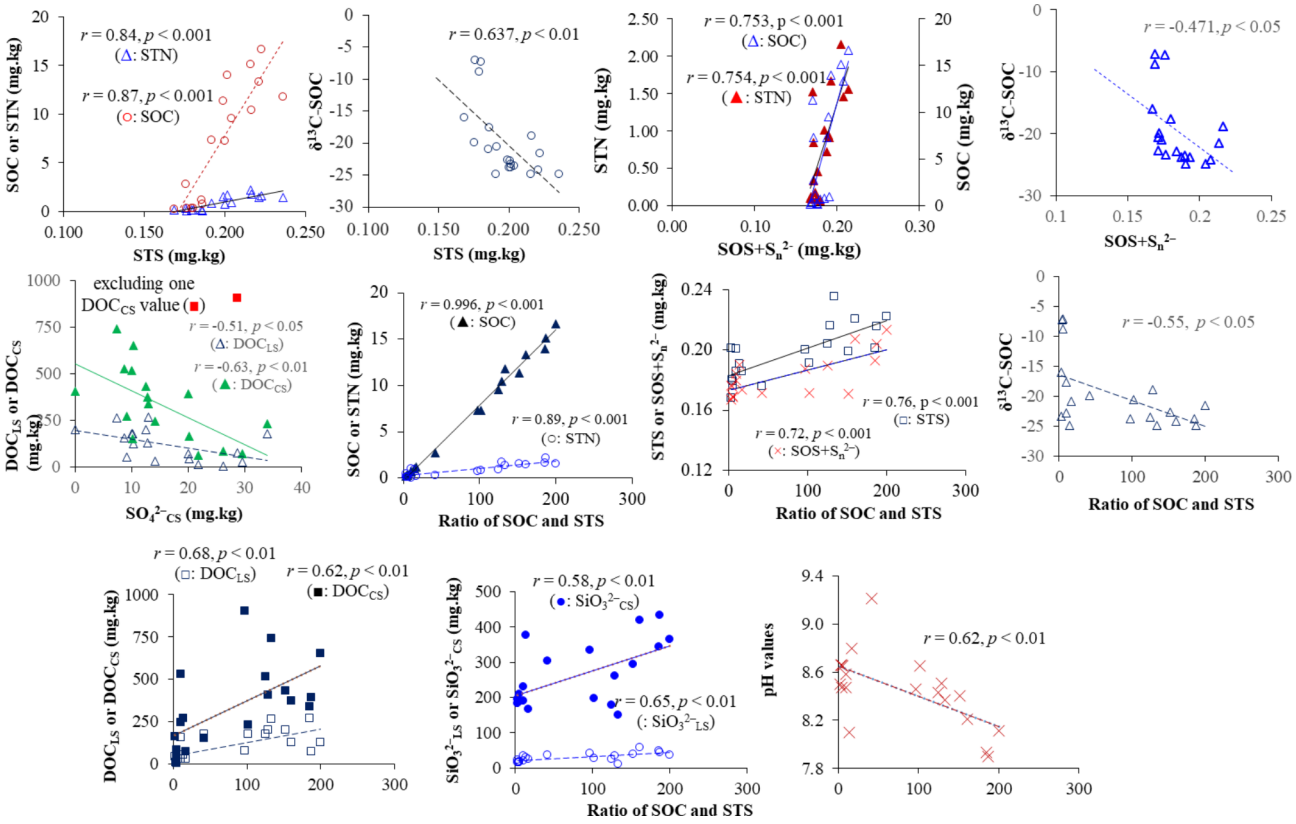

Fig. 5. Pearson correlations of STS, SO_4^{2-}, SOS + S_n^{2-} and SOC/STS ratios with some relevant parameters. The complete correlations between all parameters studied are presented in Table S3.

plus DOM or HS. Furthermore, STS showed a significant positive correlation with $SO_4^{2-}{}_{LS}$ and a negative correlation with $SO_4^{2-}{}_{CS}$ (Table S3), which suggests that increasing STS via COS sequestration by lichen-associated cyanobacterial-fungal symbioses[53,54,57] would increase the $SO_4^{2-}{}_{LS}$ content that might be exported during DOM-bound mineral dissolution or mineralization via microbial $SO_4^{2-}{}_{CS}$ reduction, associated with simultaneous sequestration (S^{2-}-S°) and redox processes (S°-SO_4^{2-}-S^{2-}/S_2^{2-}-SO_4^{2-})[55,56]. These results were further supported by the significant negative correlation of $SO_4^{2-}{}_{CS}$ with DOC_{LS}, which implies that DOM_{LS} might arise from the dissolution or mineralization of DOM-bound clay and/or carbonate secondary minerals via microbial sulfate reduction. Therefore, the involvement of $SO_4^{2-}{}_{CS}$ in the dissolution or mineralization of HS-bound minerals would affect the export of $SO_4^{2-}{}_{LS}$ by leaching into the ambient surface waters and groundwater, whereas SOS + S_n^{2-} would remain in the soil matrix in either mineral forms or as structural constituents of microorganisms.

STN, δ15N-STN, DON, and other nutrients

The STN content varied from 0.070 to 2.16 $g.kg^{-1}$ and showed, on average, the highest value in forest soils (1.51 ± 0.59 $g.kg^{-1}$), which was higher (by 13.0%) compared to agricultural soils > deep soils (91.6%) > grassland soils (96.4%) > desert sands (1480%). These results suggest the occurrence of biogeochemical steady-state/sequestered N in the various soil types examined[9,58], as well as the small ^{14}N loss via N_2O or N_2 emissions by HS-bound mineral dissolution or mineralization[9,17,18,34]. These processes are supported by the $\delta^{15}N$-PON values that, on average, were the highest in forest soils (6.21 ± 0.86‰) followed by those of agricultural soils (5.00 ± 1.69‰), grassland soils (4.29 ± 0.19‰), and deep soils (3.50 ± 1.02‰), whereas $\delta^{15}N$-PON could not be detected in desert sands, possibly due to the very low content of STN[9,17,18,34]. Lower $\delta^{15}N$ values were measured in deep soils compared to top soils, as found in previous studies[59,60], which would presumably arise from biological N fixation by specific N-fixing plant taxa[59] via various bacteria[61,62]. The highest $\delta^{15}N$ enrichment in forest soils, also reported in other studies[63], and the wide variation of $\delta^{15}N$-PON values among the top soils might be ascribed to the rapid N-bound HS mineralization or dissimilation, accompanied by the preferential loss of the light ^{14}N isotope[64] through small N_2O or N_2 emissions via denitrification[60]. These processes would produce NO_3^- with variable isotopic $\delta^{15}N$-NO_3^-[63]. The remaining parts of this subsection are presented in the SI (subsection 3.1.5.).

Discussion

Sequestration of atmospheric CO_2 in desert sands and HS-derived DIC in soils

The $\delta^{13}C$-SOC values in desert sands (-17.63 to -7.10‰, average −11.37 ± 5.05‰) were comparable with the atmospheric CO_2 content (-8.4‰ in 2015)[65], which suggests that atmospheric CO_2 can be sequestered by sand

microorganisms for their growth and metabolic respiration processes[63]. Such sequestration could for instance occur by COS uptake[11,13,55] via reduction-oxidation reactions (S^{2-}-S°-SO_4^{2-}-S^{2-}/S_2^{2-}-SO_4^{2-})[61,62] by lichen-associated cyanobacterial-fungal symbioses[33–35,65,5,6,57,70]. This interpretation is supported by the significant positive correlations of STS and SOS + S_n^{2-} with SOC, and by their negative correlations with δ^{13}C-SOC (Fig. 5; Table S3). This issue implies a simultaneous sequestration of S and C via COS uptake during photosynthesis[50,66]. Additional evidence is provided by the average SOC/S ratios in desert sands (5.7) compared to forest, agricultural, grassland, and deep soils (155–156, 75, and 9, respectively). These findings would suggest that desert sands mostly uptake atmospheric COS during photosynthesis[50,66], whereas forest, agricultural, and grassland soils would use the abundant DIC or CO_2 released from HS and DOM degradation[30,31,33]. Furthermore, the highly depleted δ^{13}C-SOC values (-24.9 to -18.8‰: average -22.7 ± 1.9‰) in the four soil types compared to desert sands (Table 1) are a key signature of sequestration/uptake of lighter CO_2 arising from plant material-derived HS and DOM in soils[33,35,67]. Notably, due to the absence of plant material-derived DIC and CO_2, the uptake of atmospheric COS would be the only pathway for microbial metabolic respiration processes and microorganisms growth in desert sands that also accounts for the observed S levels[8,37,38]. Due to the intense precipitation (445 mm in 2016) and relatively low temperature (highest temperature, 26.3–29.1°C in 2016) in Inner Mongolia (Table S2, S3), many HS components might be diagenetically produced from either terrestrial plant materials[31,32,36] or anoxygenic photosynthetically-derived SOC, by soil or sand microorganisms under wet conditions (Table S1)[31,32,36]. They would then mostly remain in a non-degraded state in soil and sand. These conditions would lead to subsequent C sequestration via organo-mineral complexes[29–31,37].

Sources of SOC and molecular composition of exported DOM and HS

The SOC basically includes soil microorganisms (e.g., bacteria, archaea, fungi, viruses, and microeukaryotes) and plant-derived materials, both of which simultaneously export DOM, HS and nutrients[8,37,38]. Specifically, SOC in desert sands mostly includes microorganisms that uptake atmospheric CO_2 for their metabolic growth/respiration, as discussed before, and no plant-derived materials. Desert autotrophic microorganisms produce HS, which EEM images and corresponding peak positions differ from those of HS isolated from other soils (Fig. 2; Table S2)[22,28,32] and rather resemble aquatic autochthonous humic-like and protein-like substances[18,68]. Desert HS would be produced rapidly and be subject to complete photochemical and microbial degradation within 24 h[18,69,70]. These effects might be the key factors for the high lability of DOC_{LS} and DOC_{CS}, as well as HS_{LS} and HS_{CS} components in desert sands. Differently, the higher fluorescence of peak M compared to peaks (C and T) in both LS- and CS-forms of FA from forest soils would suggest that individual HS components would contribute to the formation of organo-minerals as well as non-mineral states, while the highest contribution of fluorescence of LS FA peak M among all soils (Fig. 3) would suggest that there is higher export/leaching of FA_{LS} from forest soils into ambient environments.

The higher M_w and M_n values of their LS-forms compared to the CS-forms (Table 3; Figs. 1 and 3) might presumably arise from the degradation of HA_{LS}, as also indicated by the absence of fluorescence EEM peaks (Fig. 2). The significant correlation found between DOC_{LS} and DOC_{CS} (Fig. 6) would suggest that both quantities are primarily originated during the mineralization of CS-forms, as reported elsewhere[71]. These results are also supported by the predominant occurrence of HS_{LS} components with MW > 25 kDa and 15–25 kDa. Furthermore, the difference between HS_{CS} components in desert sands and other mostly plant-derived HS_{CS} was confirmed by the short-wavelength of peaks (C and A) of HA_{CS}, the degradation peak M of FA_{CS}, and the TLS peak, which resembled those of autochthonous DOM. These HS_{CS} components mostly exhibited relatively low MW (15–25 kDa and < 15 kDa, Table 3, S4) and would originate from autotrophic microorganisms, which are primarily responsible for the relatively high lability of HS_{CS}-bound organo-minerals in desert sands. The remaining parts of this subsection are presented in the SI (subsection 4.2).

The role of natural and anthropogenic processes

The key natural and human processes and factors occurring in soils primarily include sunlight-induced photochemical reactions, temperature, precipitation, microbial reactions, types of plant materials, ploughing, and cultivation (Table S5;[26,35,39]. Specifically, high contents of DOC_{LS} and DOC_{CS} in agricultural soils compared to other soil types and sands are primarily attributed to human activities (e.g., tilling, ploughing) which can subsequently influence the lability and export of DOM in LS-form, as well as the stability of organo-minerals. Due to the absence of plants in desert sands, sunlight plays a dual role, i.e., photosynthetic uptake of atmospheric CO_2 by sand autotrophic microorganisms[37,38,72] and simultaneous photodegradation of DOM and HS (produced by autotrophic microorganisms upon photosynthesis and further metabolic processing) via photoinduced generations of ROS[39], as well as microbial neoformation of DOM and HS-bound organo-minerals[2,73].

In the case of deep soils, only microbial degradation would occur due to the absence of sunlight, while in forest, agricultural, and grassland soils the effect of sunlight would be operational but only in the top layers, where photosynthetically- and microbially-derived SOC might be produced under high humidity[6,37,74,75]. In particular, the DOM or HS originated from plant materials in these soil types would cause both organic C stabilization by neoformation of organo-minerals[29–31] as well as simultaneous photochemical and microbial degradation, with final generation of DIC_{LS} and DIC_{CS}, DIN_{LS} and DIN_{CS}, DON_{LS} and DON_{CS}, $PO_4^{3-}{}_{LS}$ and $PO_4^{3-}{}_{CS}$, and $SiO_3^{2-}{}_{LS}$ and $SiO_3^{2-}{}_{CS}$ (Figs. 1 and 4). In particular, the LS-forms would be partly exported into the surrounding environments (groundwater, surface waters, and air in gaseous forms, e.g. CO_2, NO_x), whereas a portion of LS-forms and CS-forms would contribute to the neoformation of organo- and/or carbonate minerals[29–31].

Sources of SIC and DIC_{LS}/DIC_{CS}, and mineral neoformation

The highest average content of SIC in grassland and deep soils acted as the main storage of SIC. In particular, the high SIC content in deep soils might be considered a potential signature of inorganic C sequestration/

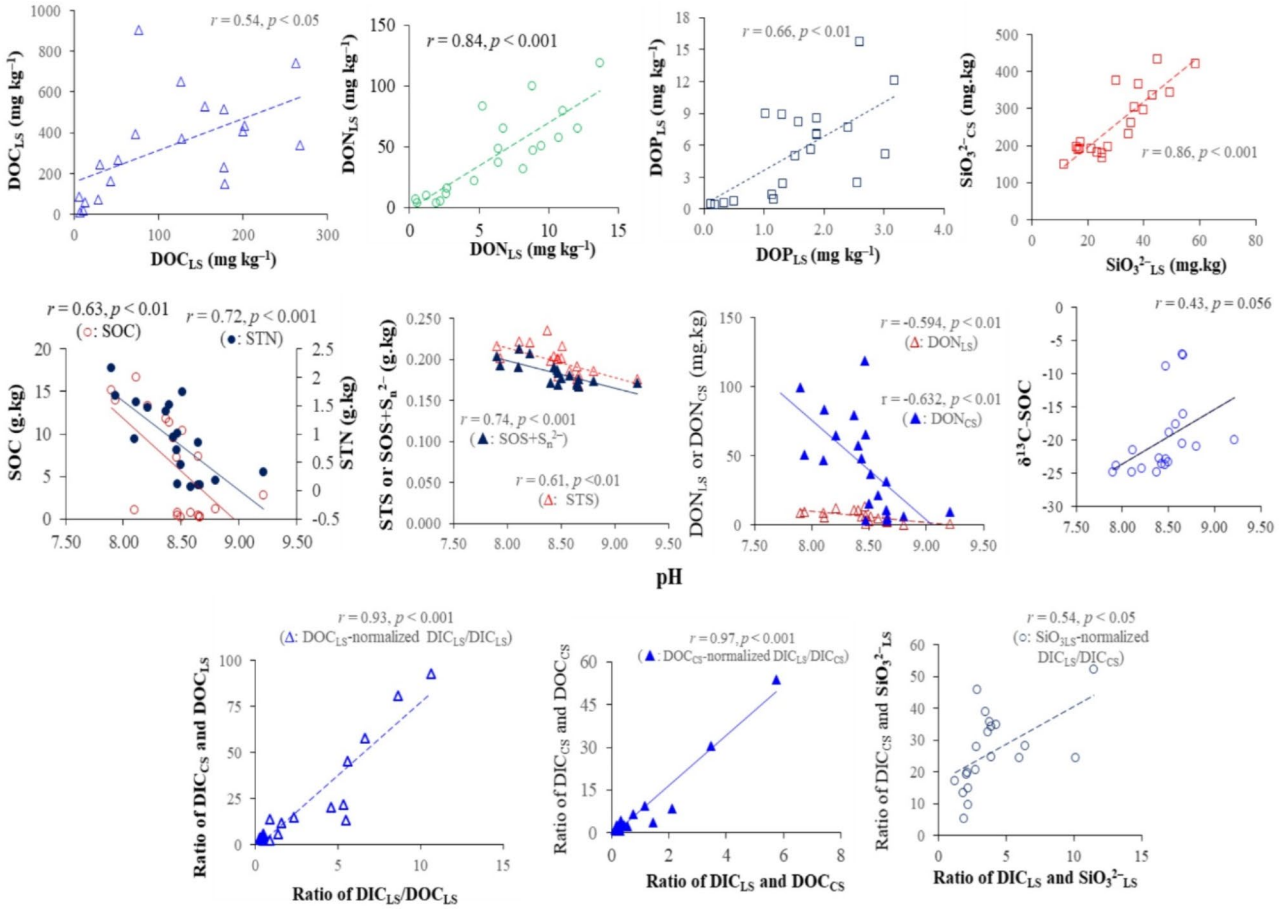

Fig. 6. Pearson correlations between some most important parameters. The significance of the *p*-values are presented at the level $p < 0.01$ and $p < 0.001$. The complete correlations between all parameters studied are presented in Table S3.

storage as carbonate minerals[33–35]. The low SOC vs. high SIC content in deep soils, desert sands, and grasslands might be due to SOC heterotrophic microbial mineralization and subsequent generation of CO_2 or SIC in deep soils[14,15,45,76–78], where CO_2 is sequestered in the form of clay and carbonate minerals[14,45,76,77]. In particular, an intense microbial mineralization of SOC in grassland soils is further supported by the relatively enriched δ^{13}C-SOC values (-20.05 ± 0.9‰) compared to those in forest and agricultural soils (23.77 ± 0.88‰ and − 23.53 ± 1.41‰, respectively).

The observed, high occurrence of DOC_{LS} and DOC_{CS} in agricultural soils (Fig. 1) and their subsequent mineralization via heterotrophic respiration and microbial sulfate reduction[14,79] would lead to the generation of DIC or CO_2[15,16,34] and to highly labile DIC_{LS}, which would undergo sequestration in CS forms via neoformation of carbonate minerals[53,54,57]. However, the long-term mineralization of DOC_{LS} and DOC_{CS} in deep soils would lead to the generation of DIC_{LS} or DIC_{CS}, which implies, respectively, the highest DIC_{LS} lability and the second highest organo-mineral neformation via DIC_{CS} in deep soils.

The δ^{13}C-SOC values measured in the soils and sands analyzed in this study (Table 1, S1), as well as in other studies, i.e., -27.7 ± 0.1‰ to -23.6 ± 0.3‰ during 3-180 days incubation and − 20.0 to -16.4 at 0–10 cm in forest and croplands[33,34], in comparison with atmospheric CO_2 (-8.4‰;[65], suggest that photosynthetic microorganisms would mostly uptake the lighter/depleted^{13}C-DIC or CO_2 from soil. In contrast, desert sands collected from three sites where plants were completely absent (δ^{13}C-SOC, -7.1‰ to -8.8‰), could uptake CO_2 exclusively from the atmosphere, whereas the sandy soils (sand fraction, 96.79–99.96%; Table 1, S1) collected from two newly-planted nearby sites, following the desert afforestation program[80] and relatively depleted in δ^{13}C-SOC (-17.6 to -16.0‰) would uptake CO_2 from both atmosphere and (depleted) plant-derived DIC or CO_2. Therefore, desert sands could act as an effective sink of atmospheric carbon via carbonate formation[81].

Differently, all other soil types featuring^{13}C-SOC values from − 24.9‰ to -18.8‰ (Table 1) would mostly uptake highly available DIC and CO_2 derived from plant materials. Especially, grassland soils, which were relatively rich in sand (82.93–85.70%) and thus relatively rich in^{13}C-SOC (-18.8 to -20.9‰), might uptake both atmospheric CO_2 and DIC and CO_2 from plant-derived DOM degradation[15,16,31]. Actually, enriched DIC and CO_2 might originate from either emission of lighter or depleted CO_2 into the atmosphere[15,16], or carbonate mineral neoformation[38,53,57]. These findings are further supported by the significant positive correlation of δ^{13}C-

SOC values with the soil sand fraction and DIC_{CS} (Table S3), which also implies that the uptake of DIC and CO_2 would involve CS-forms at the mineral-microbes interface during oxygenic/anoxygenic photosynthesis[38,53,57]. The occurrence of three processes (emission of CO_2 to the atmosphere, carbonate mineral neoformation, and DIC uptake during photosynthesis) would primarily affect SIC storage, so that DIC_{LS} and DIC_{CS} did not show any significant correlation with SIC (Table S3). The remaining parts of this subsection are presented in the SI (subsection 4.4.).

pH-dependent lability and stability of minerals

The pH values showed significant negative correlations with SOC, STN, STS, and $SOS + S_n^{2-}$ for all soil types (Fig. 6; Table S3), which suggests the occurrence of pH-dependent C, N, and S sequestration, and of S in organo-mineral and sulfide forms, i.e., the lower the pH, the higher the sequestration and vice versa. In particular, the pH-dependent sequestration was primarily due to the increasing stability of mineral forms with increasing pH, whereas a decreasing pH would produce minerals destabilization[40,82,83]. The significant negative correlations of pH with $SiO_3^{2-}{}_{LS}$, $SiO_3^{2-}{}_{CS}$, $NH_4^+{}_{CS}$, and $NO_3^-{}_{LS}$ (Table S3) suggests high availability of these nutrients at low pH and vice versa. N- and P-nutrients would be extensively generated at low pH conditions, which is also supported by the significant negative correlations of pH with DON_{LS}, DON_{CS}, and DOP_{CS} (Fig. 6; Table S3), in agreement with a previous study[84]. Furthermore, the significant positive correlation of pH with δ^{13}C-SOC (Fig. 6; Table S3) would suggest that sequestration of lighter δ^{12}C-SOC is favored at low pH conditions, while sequestration of enriched δ^{13}C-SOC would be enhanced at high pH. These results provide a novel understanding of the export and sequestration dynamics of water-extractable DOC_{LS}-normalized DIC_{LS} (and CO_2) in soils.

Sequestration of STS and $SOS + S_n^{2-}$, and redox processses involving $SO_4^{2-}{}_{LS}$ and $SO_4^{2-}{}_{CS}$

The significant positive correlations of STS with both SOC and STN for all soil types studied (Fig. 5; Table S3) suggest that S sequestration could occur simultaneously with C and N sequestration in soils and sands. Similar results, i.e., the continuous STS increase with simultaneous C and N sequestration, were obtained under sunlight and microbial dark/control conditions for 150 consecutive days, whereas other authors have reported specific sequestration of S[11–13], C[8,37], and N[9,10] under either oxygenic or anoxygenic photosynthesis[5,6,85]. These processes usually occur by lichen-associated cyanobacterial-fungal symbioses in soils[5,6,49,85]. The sequestration process is further supported by another experimental study conducted on forest (haplic luvisol) soil where a net increase in STS ranging from 1.2 to 41.0% and STN from 1.7 to 7.0% was measured under sunlight, dark, and control conditions[86]. Similarly, a net increase in SIC ranging from 3.1 to 10.1% was measured during the 0–75 day period under sunlight, and a 2.5% increase occurred during the 0–30 day period under dark conditions. Simultaneously, a net increase in SOC was measured only under sunlight (0.80%) and control (0.40%) conditions during the 75–150 day period following mineralization, with decreases of 1.8–2.4% and 2.3–6.0% over the initial 0–75 days. Notably, SOC sequestration under both sunlight and dark conditions simultaneously offsets microbial respiration, which contributes to the low carbon sequestration. Note that three experimental protocols—sunlight, dark, and control—were implemented using three aliquots of approximately 50 g each of homogeneously mixed, 2-mm sieved soil contained in 500 mL quartz bottles during the incubation periods of 0, 30, 75, and 150 days. The sunlight and dark samples were placed on the roof of a building at Tianjin University in Tianjin, China, while the control samples were maintained in a thermostat at a constant temperature of 25 °C[86].

Sulfur sequestration was further supported by the significant negative correlations of STS and $SOS + S_n^{2-}$ with δ^{13}C-SOC (Fig. 5; Table S3), implying that lower sequestration of organic and mineral S might be associated with sequestration of enriched CO_2, and the reverse. Furthermore, STS correlated significantly and positively with DOC_{LS}, DOC_{CS}, DON_{LS}, DON_{CS}, DOP_{LS}, and DOP_{CS}, thereby suggesting that increasing soil S would increase both LS- and CS-forms of organic N- and P-bound DOM, and vice versa. Soil S could thus control the occurrence of DOM and the photochemical and microbial degradative generation of its N- and P-nutrients, based on mutual positive correlations (Table S3). Most importantly, $SO_4^{2-}{}_{CS}$ showed significant negative correlations with DOC_{LS} and DOC_{CS} (Fig. 5), which suggest that SO_4^{2-}-mediated microbial reduction would mostly be responsible for the microbial mineralization of DOM, and in particular for the mineralization of SOC-derived HS-bound clay, Fe, and LDHs-like minerals via redox reactions[5,6,49,85]. The substantially lower SOC/S ratios in desert sands (5.6 ± 3.0) and deep soils (9.0 ± 6.0) compared to other soil types (72 ± 52–155 ± 42) are a key indicator of the substantially higher C and S sequestration in desert sands and deep soils compared to the other soil types. Furthermore, the significant positive correlations of SOC/S ratios with SOC, STN, STS, $SOS + S_n^{2-}$, DOC_{LS}, DOC_{CS}, $SiO_3^{2-}{}_{LS}$, and $SiO_3^{2-}{}_{CS}$ (Fig. 5) suggest the occurrence of C, S, and N sequestration, as well as their lability and/or stability via concurrent mineralization of mineral-associated components by STS-induced redox processes.

Finally, organic and mineral S ($SOS + S_n^{2-}$) contents showed significant positive correlations with SOC and STN for all soil types studied (Fig. 5), suggesting that organic and mineral S sequestration would also occur during the uptake of C and N. The persistent influence of STS or SO_4^{2-}-mediated redox processes[13,55,56,87] in the various soils, and even in desert sands, would imply that soil biogenic components always remain in a steady-state during the overall degradation processes. Therefore, S could play an important role in controlling biogenic components in soils and sands.

Materials and methods

Sampling sites and soil/land types

The sampling sites are located in the southeastern edge of the Gobi desert, Inner Mongolia Autonomous region, China (40°14′-41°08′N, 109°56′-111°42′E). This region features a typical semi-arid and temperate continental climate, strongly affected by the East Asian monsoon and characterized by relatively intense precipitations, relatively short summers with relatively moderate temperatures and a long, extremely windy and cold winter

season (Table S5). The temperature data of the tast 10 years (2012–2022) (Inner Mongolia Statistical Yearbook, 2022, http://tj.nmg.gov.cn) show an increasing trend of the summer peak temperatures since 2019, which reached the highest values of 25.6 in 2019 to 33.1°C in 2022 (Table S5). At the same time, winter temperatures are becoming progressively less rigid and ranged from the lowest value of -29.1°C in 2016 to -22.0°C in 2022. Very reasonably, these temperature variations might be affected by climate change. At the same time, annual precipitation in the 2012–2022 period showed relatively low variations, ranging from 500.3 mm in 2012 to 308.5 mm in 2017 with an average of 412.3 ± 53.5 mm.

The main soil types in Inner Mongolia are chestnut soils, as classified by Chinese standards, which were developed from Aeolian sediments. This classification is further aligned with the World Reference Base for soil resources (WRB; Table S1). The soil grounds are characterized by a high content of sand, ranging from 60 to 75% [88]. Notably, half of the region typically suffers from desertification that affects negatively about 90% of the local population, due to its secondary effects[89]. In particular, climate change and human activities (e.g., afforestation, deforestation, cropland and settlement expansion, overgrazing by livestock) and their interactions are considered the key responsible for desertification and land degradation in Inner Mongolia[90]. Other land types of the region include saline-alkali lands (0.59%), wetlands (5.08%), and unused lands (11.51%).

Soil samples

A total of 20 soil samples were collected in late October 2016 in the Inner Mongolia region, i.e., four soil samples from each of forested land, agricultural land, and grassland, three samples from deeper soil layers, and five samples from the Gobi desert sandy areas (Fig. S1). In particular, deep soils include a forest site with a depth of 1 m and two desert sand sites with depths of 1 m and 5 m, respectively. The sampling sites were selected by adopting the principle of sampling far away from the highways, to minimize human influence. Approximately 1 kg of top soil/sand (0–15 cm) was randomly collected from each sampling site using a 10-cm diameter stainless steel auger, after removing manually plant litters, roots, grasses, and debris, as described previously[28]. Three subsamples for each sample was then mixed homogeneously to obtain a spatially representative sample at the field scale. Soil samples were then oven dried at 40 °C, passed through a 2-mm sieve, ground in a mortar to yield particle sizes lower than 0.20 mm, and stored at -20 °C until further use.

Forest soils, primarily planted with coniferous and deciduous broad-leaved trees, cover approximately 22% of total land (Inner Mongolia Statistical Yearbook, 2022, http://tj.nmg.gov.cn). Agricultural lands cover approximately 4.7% of total land, with the principal crops grown being beetroots, potatoes, tomato, cereal, wheat, rice, soybean, and tubers. Grasslands cover about 36.9% of the total, with the predominance of two grassland types, i.e., shrub 5–30% and herb 5–25% [91]. The sandy desert covers 13% of total land, from which three samples were collected, one from bare sand (0–15 cm) and two (ID-4 and ID-7) from a nearby two-three years planted site. Desert afforestation via plantation in Inner Mongolia is a top priority of the Chinese Government, because afforestation in this area has potential advantages for dust mitigation and carbon sequestration[80].

Water and alkaline extracts of soil samples

A novel method[28], based on soil extraction with water first, and then with a 0.1 M NaOH solution was applied to separate the labile state (LS) from the complexed state (CS) soil components. The two extracts were obtained by several subsequent steps (Fig. S2). In the first step, ultrapure water (18.2 MΩ·cm, Mill-Q, Millipore) was added to each ground and sieved soil sample at a 1:10 soil: water ratio, the mixture was vortexed for 1 min in closed 500-mL brown bottles, shaken for 6 h at 25 °C, and then centrifuged for 20 min at 4000 rpm using a Thermo Fisher Scientific SORVALL ST 16 centrifuge, to remove suspended solids. The supernatant solution was then filtered through a 0.45-µm membrane filter (GF/F type, Shanghai Xin Ya Purification Equipment Co. Ltd, China), whereas the remaining solid residue was extracted again (repeating all the above procedure) with fresh ultrapure water for 1 h. We thus obtained a supernatant solution that was mixed with the previous one and stored in a freezer at − 20 °C until further processing. This solution represented the soil water extract (W_e).

In the second step, the soil residue after water extraction was subjected to alkaline extraction under N_2, with a 0.1 M NaOH solution at 1:10 soil residue: alkaline solution ratio, by shaking for 3 h at 25 °C. The mixture was then centrifuged as described above, and the supernatant solution was filtered through a 0.45-µm membrane filter (polytetrafluoroethylene membrane, PTFE, Shanghai Xin Ya Purification Equipment Co. Ltd, China). The remaining solid residue was extracted again with a fresh alkaline solution for 3 h, and the procedure described above was applied again to obtain another supernatant solution. The latter was mixed with the previous one to obtain the alkaline extract (A_e), and stored in a freezer at − 20 °C until further processing.

All glass bottles used for extraction purposes were soaked with 10% HNO_3 and HCl for 24 h before use, rinsed with Mill-Q (MQ) water, and then placed in a muffle furnace for 4 h at 550 °C, in order to remove any residual organic impurity. Similarly, each glass fiber filter was individually wrapped in an aluminum foil and then placed in a muffle furnace for 4 h at 550 °C, in order to remove any organic and inorganic impurities.

The W_e and A_e extracts thus contained, respectively, the water-extracted LS soil components (i.e., DOC_{LS}, HS_{LS}, ${NO_3}^-{}_{LS}$, ${NH_4}^+{}_{LS}$, ${NO_2}^-{}_{LS}$, ${PO_4}^{3-}{}_{LS}$, ${SiO_3}^{2-}{}_{LS}$, and ${SO_4}^{2-}{}_{LS}$) and the alkali-extracted CS components (i.e., the corresponding DOC_{CS}, HS_{CS}, ${NO_3}^-{}_{CS}$, ${NH_4}^+{}_{CS}$, ${NO_2}^-{}_{CS}$, ${PO_4}^{3-}{}_{CS}$, ${SiO_3}^{2-}{}_{CS}$, and ${SO_4}^{2-}{}_{CS}$). A small portion of W_e and A_e was kept at 4 °C and then analyzed for the HS fractions by fluorescence, absorbance, and DOC within 48 h, whereas the residual main portions of W_e and A_e were kept at − 20 °C for further analysis of other parameters. In particular, because both W_e and A_e contained high DOC, these solutions were diluted to reasonable absorbance values[92] before measuring fluorescence and other parameters.

Analytical methods

Physical and chemical analyses of soils

Soil water content was measured gravimetrically in triplicate, in an oven dryer at 40 °C. The pH and EC values were measured in 1:2.5 slurries of soil and ultrapure water, using a pH meter (Multi 3630 IDS, Germany) equipped with a combined glass electrode[93]. Soil total carbon (STC) and soil total nitrogen (STN) were determined on approximately 20 mg of dried, ground, and homogenized sample contained in a clean, carbon-free pre-combusted tin boat, placed on the autosampler rack assembly of an Elemental Analyzer (Elemental Vario EL cube, Germany). Soil organic carbon (SOC) was analyzed by an Elemental Analyzer on dried, ground and homogenized samples pretreated with 1 M HCl placed in a vial on an autosampler tray reported elsewhere[4]. We used sulfanilamide as a standard after every ten measurements. Soil texture/particle size distribution was determined using the hydrometer method (Master sizer 3000, Malvern). The classification of soils was referred to the WRB Texture Classes, i.e., sand (63–2000 µm), silt (2–63 µm), and clay (< 2 µm).

Stable carbon ($\delta^{13}C$) and nitrogen ($\delta^{15}N$) isotopes were measured, respectively, on approximately 2.0 mg and 30.0 mg of < 0.2-mm-ground soil samples, contained in a tin boat placed on the autosampler rack assembly of an Elemental Analyzer (Flash 2000 HT), interfaced with a Stable Carbon Isotope Ratio Mass Spectrophotometer (MAT 253 Plus, Thermo Fisher, Germany). For the $\delta^{13}C$ analysis of SOC, carbonates were removed with an excess of HCl (2 M). The IAEA-600 Caffeine was used as $\delta^{13}C$ standard, and both IAEA-600 Caffeine and USGS 40 & 41 L-Glutamic Acid were used as $\delta^{15}N$ standard. All results were expressed in delta notation (Eq. 1):

$$\delta^{13}C \text{ or } \delta^{15}N = \left[\left(\frac{R_{\text{sample}}}{R_{\text{std}}}\right) - 1\right] \times 1000 \quad (1)$$

where R_{sample} and R_{std} are the absolute ratios of $\delta^{13}C/\delta^{12}C$ or $\delta^{15}N/\delta^{14}N$ for sample and standard, respectively. $\delta^{13}C$ and $\delta^{15}N$ values are expressed in parts per thousand (‰) relative to the Vienna Pee Dee Belemnite (VPDB) international reference[94].

Analyses of W_e and A_e

Dissolved organic carbon (DOC) and dissolved inorganic carbon (DIC) The concentrations of DOC and DIC were measured by an Aurora combustion total organic carbon (TOC) auto-sampler analyzer (O.I. Analytical Aurora, Model 1030, USA). An aliquot of sample was transferred to the reaction chamber and added with a predetermined volume of H_3PO_4. The acidified sample ($pH \leq 2$) was heated at a temperature that is able to decompose carbonates and bicarbonates to CO_2. After the reaction was completed, TIC was detected.

After removing TIC, the strong oxidizing agent $Na_2S_2O_8$ was added, which reacts quickly with organic C at 100 °C to generate CO_2. At least three injections were performed for each DOC and DIC analysis. Sodium carbonate was used as the DIC standard solution and potassium hydrogen phthalate as the DOC standard solution. Before measurement, the instrument was calibrated with the standard at concentrations of 1, 2, 5, 10, and 20 ppm. Quality control and quality assurance were estimated by determining the contents in blank or standard reference materials.

Nutrients Total nitrogen (TN), nitrate (NO_3^-), nitrite (NO_2^-), ammonia (NH_4^+), total phosphorus (TP), dissolved inorganic phosphate (DIP: PO_4^{3-}) and silicate (SiO_3^{2-}) concentrations were measured colorimetrically within 72 h from extraction, using an automated continuous flow analyzer (Skalar San++System). The concentrations of dissolved inorganic nitrogen (DIN), dissolved organic nitrogen (DON), and dissolved organic phosphorus (DOP) were calculated by using Eqs. 2 and 3.

$$\text{DON} = \text{TN} - \text{DIN}\ (\text{NO}_3^- + \text{NO}_2^- + \text{NH}_4^+) \quad (2)$$

$$\text{DOP} = \text{TP} - \text{DIP} \quad (3)$$

Fluorescence EEM measurement and PARAFAC modeling The excitation emission matrix (EEM) fluorescence spectra were acquired by a fluorescence spectrophotometer (F-7000, Hitachi, Japan), equipped with a 700-W xenon lamp as the excitation source. The response time was set at 0.5 s and the slit widths of excitation and emission were set at 5 nm. The excitation wavelength was scanned from 220 to 450 nm at a scan speed of 1200 nm min^{-1} and increments of 5 nm, whereas the emission wavelength was recorded from 280 to 550 nm at 1-nm intervals[93]. Ultrapure water (18.2 Mill-Q) used as a blank was scanned before sample analysis and after every ten samples, to check the instrument performance and ensure data quality. The EEM spectrum of ultrapure water was subtracted from the EEM spectrum of each sample. A quinine sulfate (QS) solution of 4 µg L^{-1} in 0.01 N H_2SO_4 was used to normalize fluorescence, and the fluorescence intensities were calibrated using the intensity of the QS peak at Ex/Em = 350/450 nm (1 µg/L = 1 QS unit, QSU)[95].

The well-known scattering effect that appears when a high concentration of DOM (> 15–30 mg/L) is present in the sample requires the fluorescence spectra to be measured at low DOM concentrations (~ 10 mg/L)[96–99]. Furthermore, the inner-filter correction was obtained by diluting the analyte solution at a fixed absorbance value (0.1 cm^{-1}) of the Ex wavelength. In particular, a satisfactory correction of primary and secondary inner filter effects can be achieved when the absorbance at the Ex wavelength of 254 nm is below approximately 0.3 cm^{-1} [100]. In this work, to avoid inner-filter effects and fluorescence quenching, fluorescence was measured after diluting the analyte solutions with reference to the initially measured DOC concentration[32]. Furthermore, each fluorescence peak intensity was rechecked and corrected using the common absorbance-based approach[92].

Parallel factor (PARAFAC) analysis was conducted on preprocessed EEM data using the N-way Toolbox for MATLAB[101], described elsewhere[102]. First, Rayleigh and Raman peaks as well as the spectrum of an

ultrapure water blank were subtracted from the experimental EEM spectra, using a homemade Excel program[28]. Afterwards, to avoid mixing of fluorescent components of different samples that might produce artifacts, PARAFAC analysis was performed on each soil sample by the appropriate procedures[28,103]. Finally, non-negative constraints were applied to the PARAFAC model. The detailed procedure used for PARAFAC modeling of EEM spectra is reported elsewhere[28,103].

High-performance size-exclusion chromatography (HPSEC) The M_w profiles were measured by a Shimadzu High Performance Liquid Chromatograph (HPLC) using an Acclaim Mixed-Mode HILIC-1 chromatographic column that was equilibrated at 25 °C. An aliquot of 100 µL of each W_e and A_e sample was injected, after previous filtration through a 0.45-µm membrane filter. The mobile phase used was a mixture of $Na_2HPO_4{\cdot}12H_2O$ and $NaH_2PO_4{\cdot}2H_2O$ at a concentration of 0.02 mol/L, adjusted to an ionic strength of 0.1 mol/L with sodium chloride. The mobile phase flow rate and the sample volume were set, respectively, at 0.5 mL/min and 100 µL. The wavelength of the UV detector was set at 254 nm.

An important issue in the determination of the relative MW by HPSEC is to select a calibration compound with shape and structure similar to that of the molecule to be measured. In studying the relationship between the MWs of standards and samples, Chin et al.[104] found that the molecular configuration of polystyrene sulfonate standards (PSS) was the most similar to that of HS, a significant constituent of DOM in natural environments. Based on previous research results, a number of polystyrenes of appropriate MWs (1100, 3610, 5580 and 33400 Da) were selected in this experiment, to construct a calibration curve and determine the relationship between retention time and MW (Fig S3).

Compared to the ultrafiltration method to measure the MW of DOM, HPSEC has the advantages of simple sample pretreatment process, lower dosage (< 100 µL), rapidity (~ 15 min), good reproducibility, and high sensitivity. In addition, HPSEC could simultaneously provide the weight-averaged molecular weight (M_w), the number-averaged molecular weight (M_n), and the polydispersity coefficient ρ that represents the degree of dispersion of the MW distribution of DOM. The M_w, M_n, and ρ values were calculated from the HPSEC-UV chromatograms according to Eqs. 4–6 [105].

$$M_w = \frac{\sum_{i=1}^{n} (h_i \cdot Mw_i)}{\sum_{i=1}^{n} h_i} \tag{4}$$

$$M_n = \frac{\sum_{i=1}^{n} h_i}{\sum_{i=1}^{n} \left(\frac{h_i}{Mw_i}\right)} \tag{5}$$

$$\rho = \frac{M_w}{M_n} \tag{6}$$

where h_i is the height of the chromatogram at the elution time i, MW_i is the apparent MW in Da corresponding to the elution time i, and n is the number of data points. The apparent M_w values were estimated from the calibration curve in the elution time range 3.0–10.0 min, for which an excellent fitting equation was achieved. Thus, the calculated M_w, M_n, and ρ did not consider the fraction below an elution time of 3 min (biopolymers), whereas a minor fraction appeared at elution times between 3 and 8 min (neutrals) (Fig. 3S).

GIS and statistical analysis

The ArcGIS (ArcMap 10.5) method was used to locate the spatial distribution of sampling sites. All data were subjected to the analysis of variance (ANOVA) and Pearson correlation analysis (PCA), using the SPSS21.0 software. The significance levels were reported as significant at $p < 0.05$ and highly significant at $p < 0.01$. Data were analyzed by multivariate analysis and descriptive statistics, using the Origin 2018 software. Figures were plotted using Origin 2018 and GraphPad Prism 9.

Data availability

All data is provided within the manuscript or supplementary information files.

Received: 31 May 2024; Accepted: 14 November 2024
Published online: 18 November 2024

References

1. Hemingway, J. D. et al. Mineral protection regulates long-term global preservation of natural organic carbon. *Nature* **570**, 228–231 (2019).
2. Kleber, M. et al. Dynamic interactions at the mineral–organic matter interface. *Nature Reviews Earth & Environment* **2**, 402–421 (2021).
3. He, W., Jung, H., Lee, J. H. & Hur, J. Differences in spectroscopic characteristics between dissolved and particulate organic matters in sediments: Insight into distribution behavior of sediment organic matter. *Sci. Total Environ.* **547**, 1–8 (2016).
4. Olk, D. C. et al. Environmental and agricultural relevance of humic fractions extracted by alkali from soils and natural waters. *J. Environ Qual* **48**, 217–232 (2019).
5. Loron, C. C. et al. Early fungi from the proterozoic era in Arctic Canada. *Nature* **570**, 232–235 (2019).
6. Heckman, D. S. et al. Molecular evidence for the early colonization of land by fungi and plants. *Science* **1979**(293), 1129–1133 (2001).
7. Protoschill-Krebs, G. & Kesselmeier, J. Enzymatic pathways for the consumption of carbonyl sulphide (COS) by higher plants. *Botanica Acta* **105**, 66 (1992).

8. Wohlfahrt, G., Fenstermaker, L. F. & Arnone Iii, J. A. Large annual net ecosystem CO_2 uptake of a Mojave Desert ecosystem. *Glob Chang Biol* **14** (2008).
9. Levicán, G., Ugalde, J. A., Ehrenfeld, N., Maass, A. & Parada, P. Comparative genomic analysis of carbon and nitrogen assimilation mechanisms in three indigenous bioleaching bacteria: Predictions and validations. *BMC Genomics* **9** (2008).
10. Ueki, T. & Lovley, D. R. Genome-wide gene regulation of biosynthesis and energy generation by a novel transcriptional repressor in Geobacter species. *Nucleic Acids Res* **38** (2009).
11. Kelly, B. *et al.* Sulfur sequestration promotes multicellularity during nutrient limitation. *Nature* **591** (2021).
12. Kesselmeier, J., Teusch, N. & Kuhn, U. Controlling variables for the uptake of atmospheric carbonyl sulfide by soil. *Journal of Geophysical Research Atmospheres* **104** (1999).
13. Mcrose, D. L. & Newman, D. K. Redox-active antibiotics enhance phosphorus bioavailability. *Science 371* (2021).
14. Bond-Lamberty, B. & Thomson, A. Temperature-associated increases in the global soil respiration record. *Nature* **464**, 579–582 (2010).
15. Huang, W. & Hall, S. J. Elevated moisture stimulates carbon loss from mineral soils by releasing protected organic matter. *Nat Commun* **8** (2017).
16. Melillo, J. M. *et al.* Long-term pattern and magnitude of soil carbon feedback to the climate system in a warming world. *Science 358* (2017).
17. Barrón, V. *et al.* Photochemical emission and fixation of NOX gases in soils. *Science of the Total Environment* **702** (2020).
18. Yang, X. et al. New insights into mechanisms of sunlight- and dark-mediated high-temperature accelerated diurnal production-degradation of fluorescent DOM in lake waters. *Science of the Total Environment* **760**, 143377 (2021).
19. Meredith, L. K. *et al.* Coupled biological and abiotic mechanisms driving carbonyl sulfide production in soils. *Soil Syst* **2** (2018).
20. Drake, T. W. et al. Mobilization of aged and biolabile soil carbon by tropical deforestation. *Nat Geosci* **12**, 541–546 (2019).
21. Chupakov, A. V. *et al.* Export of organic carbon, nutrients and metals by the mid-sized Pechora River to the Arctic Ocean. *Chem Geol* **632** (2023).
22. Gao, L., Zhou, Z., Reyes, A. V. & Guo, L. Yields and characterization of dissolved organic matter from different aged soils in Northern Alaska. *J Geophys Res Biogeosci* **123**, 2035–2052 (2018).
23. Mostofa, K. M. G. *et al.* Continuous production-degradation of dissolved organic matter provides signals of biogeochemical processes from terrestrial to marine end-members. *Frontiers in Marine Science*. https://doi.org/10.3389/fmars.2022.1044135 (2022).
24. Andersson, A. *et al.* Microbial food web changes induced by terrestrial organic matter and elevated temperature in the coastal northern Baltic Sea. *Front Mar Sci* **10** (2023).
25. Possinger, A. R. et al. Climate effects on subsoil carbon loss mediated by soil chemistry. *Environ Sci Technol* **55**, 16224–16235 (2021).
26. Lehmann, J. & Kleber, M. The contentious nature of soil organic matter. *Nature 528*, 60–68 (2015).
27. Kotzé, E., Loke, P. F., Akhosi-Setaka, M. C. & Du Preez, C. C. Land use change affecting soil humic substances in three semi-arid agro-ecosystems in South Africa. *Agric Ecosyst Environ* **216**, 194–202 (2016).
28. Mohinuzzaman, M. et al. Insights into solubility of soil humic substances and their fluorescence characterisation in three characteristic soils. *Science of the Total Environment* **720**, 1–38 (2020).
29. Vidal, A. *et al.* Visualizing the transfer of organic matter from decaying plant residues to soil mineral surfaces controlled by microorganisms. *Soil Biol Biochem* **160** (2021).
30. Craig, M. E. *et al.* Fast-decaying plant litter enhances soil carbon in temperate forests but not through microbial physiological traits. *Nat Commun* **13** (2022).
31. Islam, M. R., Singh, B. & Dijkstra, F. A. Stabilisation of soil organic matter: interactions between clay and microbes. *Biogeochemistry* **160** (2022).
32. Tadini, A. M. et al. Soil organic matter in podzol horizons of the Amazon region: Humification, recalcitrance, and dating. *Science of the Total Environment* **613–614**, 160–167 (2018).
33. Qin, C. *et al.* Vertical variations of soil carbon under different land uses in a karst critical zone observatory (CZO), SW China. *Geoderma* **412** (2022).
34. Lerch, T. Z., Nunan, N., Dignac, M. F., Chenu, C. & Mariotti, A. Variations in microbial isotopic fractionation during soil organic matter decomposition. *Biogeochemistry* **106** (2011).
35. Razanamahandry, V. F. *et al.* Stable isotope profiles of soil organic carbon in forested and grassland landscapes in the Lake Alaotra basin (Madagascar): Insights in past vegetation changes. *Biogeosciences* **19** (2022).
36. Semenov, V. M., Tulina, A. S., Semenova, N. A. & Ivannikova, L. A. Humification and nonhumification pathways of the organic matter stabilization in soil: A review. *Eurasian Soil Science* **46** (2013).
37. Schlesinger, W. H. An evaluation of abiotic carbon sinks in deserts. *Global Change Biology*. https://doi.org/10.1111/gcb.13336 (2017).
38. Liu, Z. *et al.* Desert soil sequesters atmospheric CO2 by microbial mineral formation. *Geoderma* **361** (2020).
39. Georgiou, C. D. *et al.* Evidence for photochemical production of reactive oxygen species in desert soils. *Nat Commun* **6** (2015).
40. Zhang, J. *et al.* Isolation of dissolved organic matter from aqueous solution by precipitation with FeCl3: Mechanisms and significance in environmental perspectives. *Scientific Reports 13*, 1–15 (2023).
41. Piccolo, A., Conte, P., Spaccini, R. & Mbagwu, J. S. C. Influence of land use on the characteristics of humic substances in some tropical soils of Nigeria. *Eur J Soil Sci* **56**, 343–352 (2005).
42. Mostofa, K. M. G., Yoshioka, T., Konohira, E. & Tanoue, E. Dynamics and characteristics of fluorescent dissolved organic matter in the groundwater, river and lake water. *Water Air Soil Pollut* **184**, 157–176 (2007).
43. Flemming, H. C. & Wingender, J. The biofilm matrix. *Nature Reviews Microbiology*. https://doi.org/10.1038/nrmicro2415 (2010).
44. Guidi, L. *et al.* Plankton networks driving carbon export in the oligotrophic ocean. *Nature* **532** (2016).
45. Roth, V. N. *et al.* Persistence of dissolved organic matter explained by molecular changes during its passage through soil. *Nature Geoscience 12*, 755–761 (2019).
46. Senesi, N. Molecular and quantitative aspects of the chemistry of fulvic acid and its interactions with metal ions and organic chemicals. Part II. The fluorescence spectroscopy approach. *Anal Chim Acta* **232**, 77–106 (1990).
47. Plaza, C., Brunetti, G., Senesi, N. & Polo, A. Molecular and quantitative analysis of metal ion binding to humic acids from sewage sludge and sludge-amended soils by fluorescence spectroscopy. *Environ Sci Technol* **40** (2006).
48. Mostofa, K. M. G., Liu, C. Q., Vione, D., Gao, K. & Ogawa, H. Sources, factors, mechanisms and possible solutions to pollutants in marine ecosystems. *Environmental Pollution* **182**, 461–478 (2013).
49. Jordaan, K. *et al.* Hydrogen-oxidizing bacteria are abundant in desert soils and strongly stimulated by hydration. *mSystems* **5** (2020).
50. Asaf, D. *et al.* Ecosystem photosynthesis inferred from measurements of carbonyl sulphide flux. *Nat Geosci* **6** (2013).
51. Senesi, N. Molecular and quantitative aspects of the chemistry of fulvic acid and its interactions with metal ions and organic chemicals. Part I. The electron spin resonance approach. *Anal Chim Acta* **232**, 51–75 (1990).
52. Khan, A. I. & O'Hare, D. Intercalation chemistry of layered double hydroxides: Recent developments and applications. in *Journal of Materials Chemistry* vol. 12 (2002).
53. Hilton, R. G. & West, A. J. Mountains, erosion and the carbon cycle. *Nat Rev Earth Environ* **1**, 284–299 (2020).
54. Zamanian, K., Zhou, J. & Kuzyakov, Y. Soil carbonates: The unaccounted, irrecoverable carbon source. *Geoderma* **384** (2021).

55. Lovley, D. R. Bug juice: Harvesting electricity with microorganisms. *Nat Rev Microbiol* **4**, 497–508 (2006).
56. Jørgensen, B. B. Mineralization of organic matter in the sea bed—The role of sulphate reduction. *Nature* **296** (1982).
57. Liu, Z. *et al.* Soil microbes from saline–Alkali farmland can form carbonate precipitates. *Agronomy* **13** (2023).
58. Possinger, A. R. *et al.* Organo–organic and organo–mineral interfaces in soil at the nanometer scale. *Nat Commun* **11** (2020).
59. Elliott, E. M. & Brush, G. S. Sedimented organic nitrogen isotopes in freshwater wetlands record long-term changes in watershed nitrogen source and land use. *Environ Sci Technol* **40** (2006).
60. Van Groenigen, J. W., Zwart, K. B., Harris, D. & Van Kessel, C. Vertical gradients of δ15N and δ18O in soil atmospheric N_2O—Temporal dynamics in a sandy soil. *Rapid Communications in Mass Spectrometry* **19** (2005).
61. Levy-Booth, D. J., Prescott, C. E. & Grayston, S. J. Microbial functional genes involved in nitrogen fixation, nitrification and denitrification in forest ecosystems. *Soil Biol Biochem* **75**, 11–25 (2014).
62. Vitousek, P. M. *et al.* Towards an ecological understanding of biological nitrogen fixation. in *Biogeochemistry* vols 57–58 (2002).
63. Wang, X. et al. Globally nitrogen addition alters soil microbial community structure, but has minor effects on soil microbial diversity and richness. *Soil Biol Biochem* **179**, 108982 (2023).
64. Dijkstra, P. *et al.* 15N enrichment as an integrator of the effects of C and N on microbial metabolism and ecosystem function. *Ecol Lett* **11** (2008).
65. Graven, H., Keeling, R. F. & Rogelj, J. changes to carbon isotopes in atmospheric CO_2 over the industrial era and into the future. *Global Biogeochem Cycles* **34** (2020).
66. Kaisermann, A., de Vries, F. T., Griffiths, R. I. & Bardgett, R. D. Legacy effects of drought on plant–soil feedbacks and plant–plant interactions. *New Phytologist* **215**, (2017).
67. Liu, S. et al. Cation-induced coagulation of aquatic plant-derived dissolved organic matter: Investigation by EEM-PARAFAC and FT-IR spectroscopy. *Environmental Pollution* **234**, 726–734 (2018).
68. Stedmon, C. A. *et al.* Photochemical production of ammonium and transformation of dissolved organic matter in the Baltic Sea. *Mar Chem* **104** (2007).
69. Smith, H. J. *et al.* Microbial formation of labile organic carbon in Antarctic glacial environments. *Nat Geosci* **10** (2017).
70. Shammi, M., Pan, X., Mostofa, K. M. G., Zhang, D. & Liu, C. Q. Seasonal variations and characteristics differences in the fluorescent components of extracellular polymeric substances from mixed biofilms in saline lake. *Sci Bull (Beijing)* **62**, 764–766 (2017).
71. Fang, C., Smith, P. & Smith, J. U. Is resistant soil organic matter more sensitive to temperature than the labile organic matter?. *Biogeosciences Discussions* **2**, 725–735 (2005).
72. Yang, Y. et al. Nitrogen fertilization weakens the linkage between soil carbon and microbial diversity: A global meta-analysis. *Glob Chang Biol* **28**, 6446–6461 (2022).
73. Yu, G. H. et al. Fungal nanophase particles catalyze iron transformation for oxidative stress removal and iron acquisition. *Current Biology* **30**, 2943-2950.e4 (2020).
74. Lange, O. L., Belnap, J. & Reichenberger, H. Photosynthesis of the cyanobacterial soil-crust lichen Collema tenax from arid lands in southern Utah, USA: Role of water content on light and temperature responses of CO2 exchange. *Funct Ecol* **12** (1998).
75. Hayes, M. H. B., Swift, R. S. & Knicker, H. An appreciation of the contribution of Frank Stevenson to the advancement of studies of soil organic matter and humic substances. *J Soils Sediments* **18**, 1212–1231 (2018).
76. Rousk, J., Brookes, P. C. & Bååth, E. Contrasting soil pH effects on fungal and bacterial growth suggest functional redundancy in carbon mineralization. *Appl Environ Microbiol* **75**, 1589–1596 (2009).
77. Dorrepaal, E. et al. Carbon respiration from subsurface peat accelerated by climate warming in the subarctic. *Nature* **460**, 616–619 (2009).
78. Shahzad, T. et al. Root penetration in deep soil layers stimulates mineralization of millennia-old organic carbon. *Soil Biol Biochem* **124**, 150–160 (2018).
79. Bond-Lamberty, B., Bailey, V. L., Chen, M., Gough, C. M. & Vargas, R. Globally rising soil heterotrophic respiration over recent decades. *Nature* **560** (2018).
80. Han, Y., Liu, H., Zhou, L., Hao, Q. & Cheng, Y. Postglacial evolution of forest and grassland in southeastern Gobi (Northern China). *Quat Sci Rev* **248**, 106611 (2020).
81. Stone, R. Ecosystems: Have desert researchers discovered a hidden loop in the carbon cycle? *Science* vol. 320. https://doi.org/10.1126/science.320.5882.1409 (2008).
82. Gilbert, B., Lu, G. & Kim, C. S. Stable cluster formation in aqueous suspensions of iron oxyhydroxide nanoparticles. *J Colloid Interface Sci* **313** (2007).
83. Yang, X. *et al.* Solubility characteristics of soil humic substances as a function of pH. Biogeosciences (accepted after review: Interactive Discussion. 10.5194/egusphere-2023-2994.
84. Lavallee, J. M. *et al.* Land management shapes drought responses of dominant soil microbial taxa across grasslands. *Nat Commun* **15** (2024).
85. Cohen, Y., Jørgensen, B. B., Padan, E. & Shilo, M. Sulphide-dependent anoxygenic photosynthesis in the cyanobacterium Oscillatoria limnetica. *Nature* **257** (1975).
86. Mohinuzzaman M, Z. J. M. K. S. R. Z. W. C. S. N. S. G. V. D. L. S. Y. J. and L. C. Simulated climatic warming accelerates sequestration, transformation, and export/emission of soil biogenic, redox, and non-redox components, including As and Hg. *Catena (Under review)* (2024).
87. Li, X. S. et al. Oxidation of elemental sulfur by Fusarium solani strain THIF01 harboring endobacterium Bradyrhizobium sp. *Microb Ecol* **60**, 96–104 (2010).
88. Yu, H. X. & Chen, G. Divergent changes in plant community composition under 3-decade grazing exclusion in continental steppe. *PLoS One* **6**, 26506 (2011).
89. Ding Xue. *Study on Dynamic Change of Land Desertification in Inner Mongolia*. Master degree, Northeast Agricultural University (2108).
90. Li, C. et al. Drivers and impacts of changes in China's drylands. *Nature Reviews Earth & Environment* **2**, 858–873 (2021).
91. Du, H., Li, S., Webb, N. P., Zuo, X. & Liu, X. Soil organic carbon (SOC) enrichment in aeolian sediments and SOC loss by dust emission in the desert steppe, China. *Science of the Total Environment* **798** (2021).
92. Kothawala, D. N., Murphy, K. R., Stedmon, C. A., Weyhenmeyer, G. A. & Tranvik, L. J. Inner filter correction of dissolved organic matter fluorescence. *Limnol Oceanogr Methods* **11**, 616–630 (2013).
93. Wang, R. *et al.* Characterizing the interaction between antibiotics and humic acid by fluorescence quenching method. *Int J Environ Res Public Health* **15** (2018).
94. Brand, M., Laier, C. & Young, K. S. Internet addiction: Coping styles, expectancies, and treatment implications. *Front Psychol* **5**, 1–14 (2014).
95. Mostofa, K. M. G. et al. Environmental characteristics and changes of sediment pore water dissolved organic matter in four Chinese lakes. *Environmental Science and Pollution Research* **25**, 2783–2804 (2018).
96. Yang, Y. H. & Zhang, D. H. Concentration effect on the fluorescence spectra of humic substances. *Commun Soil Sci Plant Anal* **26**, 2333–2349 (1995).
97. Nkhili, E., Guyot, G., Vassal, N. & Richard, C. Extractability of water-soluble soil organic matter as monitored by spectroscopic and chromatographic analyses. *Environmental Science and Pollution Research* **19**, 2400–2407 (2012).

98. Yu, G. H. et al. Binding of organic ligands with Al(III) in dissolved organic matter from soil: Implications for soil organic carbon storage. *Environ Sci Technol* **46**, 6102–6109 (2012).
99. Wu, Y. & Jiang, Y. A case study on the method-induced difference in the chemical properties and biodegradability of soil water extractable organic carbon of a granitic forest soil. *Science of the Total Environment* **565**, 656–662 (2016).
100. Ohno, T. Response to comment on "Fluorescence inner-filtering correction for determining the humification index of dissolved organic matter"†. *Environ Sci Technol* **36**, 4196–4196 (2002).
101. Andersson, C. A. & Bro, R. The N-way toolbox for MATLAB. *Chemometrics and Intelligent Laboratory Systems* **52**, 1–4 (2000).
102. Stedmon, C. A., Markager, S. & Bro, R. Tracing dissolved organic matter in aquatic environments using a new approach to fluorescence spectroscopy. *Mar Chem* **82**, 239–254 (2003).
103. Mostofa, K. M. G. et al. Characterization of Nanming River (southwestern China) sewerage-impacted pollution using an excitation-emission matrix and PARAFAC. *Limnology (Tokyo)* **11**, 217–231 (2010).
104. Chin, Y. P., Alken, G. & O'Loughlin, E. Molecular weight, polydispersity, and spectroscopic properties of aquatic humic substances. *Environ Sci Technol* **28**, 1853–1858 (1994).
105. Ignatev, A. & Tuhkanen, T. Step-by-step analysis of drinking water treatment trains using size-exclusion chromatography to fingerprint and track protein-like and humic/fulvic-like fractions of dissolved organic matter. *Environ Sci (Camb)* **5**, 1568–1581 (2019).

Acknowledgements

This study was supported by the National Natural Science Foundation of China (Grant No. U1612441), the Ministry of Science and Technology of China (Grant No. 2019YFC1804400) and also by the Key Construction Program of the National "985" Project, Tianjin University, China.

Author contributions

Conceptualization and Supervision: K.M.G.M., C.Q.L. Writing—original draft: K.M.G.M., N.S., X.Y. Investigation and formal analysis: X.Y., X.G. Funding acquisition: K.M.G.M., W.Z., S.L.L., C.Q.L. Validation: X.Y., X.G., K.M.G.M., W.Z., N.S., G.S.S., D.V., J.Y., S.L.L, L.L., C.Q.L. Writing-review & editing: W.Z., G.S.S., D.V., S.L.L. PARAFAC analysis: J.Y.

Declarations

Competing interests

The authors declare no competing interests.

Additional information

Supplementary Information The online version contains supplementary material available at https://doi.org/10.1038/s41598-024-80004-1.

Correspondence and requests for materials should be addressed to K.M.G.M. or C.-Q.L.

Reprints and permissions information is available at www.nature.com/reprints.

Publisher's note Springer Nature remains neutral with regard to jurisdictional claims in published maps and institutional affiliations.